

See discussions, stats, and author profiles for this publication at: <https://www.researchgate.net/publication/267715645>

AN INTRODUCTION TO ENTROPIC LATTICE BOLTZMANN SCHEME

Article

CITATION

1

READS

35

2 authors, including:



Sauro Succi

INFN - Istituto Nazionale di Fisica Nucleare

490 PUBLICATIONS 14,057 CITATIONS

SEE PROFILE



e-Lecture Notes

ISSN 1970-4429


AN INTRODUCTION TO ENTROPIC LATTICE BOLTZMANN SCHEME

Francesca Tosi¹ and Sauro Succi²

¹Dip. di Matematica "U.Dini"
Università degli Studi di Firenze,
Viale Morgagni, 67-a,
50134 Firenze, Italy
tosi@math.unifi.it

²Istituto per le Applicazioni del Calcolo CNR,
Viale del Policlinico, 137,
00161, Rome, Italy

DOI: 10.1685/SELN08004 - Vol. 1 - 2008

Licensed under  **creative commons**
Attribution-Non-Commercial-No Derivative Works

Abstract.

Recently, there has been much progress in developing the method of the lattice Boltzmann equation as an alternative, computational technique for solving complex fluid dynamic systems. Adopting a macroscopic method for computational fluid dynamics (CFD), the variables of interest, such as velocity u and pressure p , can be obtained by solving the Navier-Stokes (NS) equations.

The lattice Boltzmann models are rather different numerical techniques aimed at modeling a physical system in terms of the dynamics of fictitious particles (or mass distribution functions \mathbf{f}) and the macroscopic quantities (such as mass density and momentum density) can then be obtained by evaluating the hydrodynamic moments of the distribution function \mathbf{f} .

This method is now considered as a serious alternative to standard computational fluid dynamics. The main idea of this approach is to model the physical reality at a mesoscopic level: the generic features of microscopic processes can be expressed through simple rules, from which the desired macroscopic behavior emerges as a collective effect of the interactions between the many elementary components.

Keywords: Entropic Lattice Boltzmann scheme, Entropy production.

1. Introduction.

Fluid motion can take a wide variety of form, from simple (such as laminar flow in a pipe) to more complex flows (such as vortex around a cylinder, wave motion and turbulence) and a wide class of engineering problems are related to investigation of complex flows (such as turbulent phenomena around a vehicle). A few situations can be examined experimentally, but this approach is of difficult and expensive realization. The numerical approach prove to be advantageous in simulating flow structures experienced in the motion of fluid.

Computational fluid dynamic (CFD) has developed mainly around using numerical techniques to solve the Navier-Stokes equations (cfr. [1]). Another approach, that proves to produce good results in CFD, is the molecular dynamics approach, developed in the last decade. Indeed, one obvious way to simulate a fluid on a computer is to model the individual molecules which make up the fluid. Then, once the inter-molecular interactions between the particles are provided correctly, the system behaves as a fluid (cfr. [2]). One of the main disadvantage with such an approach is that large computer resources are required.

In the last few years an alternative numerical method has attracted much attention as a technique in fluid engineering (cfr. [3]). The basic philosophy of this model is the description of the fluid as an ensemble of many particles interacting locally at the sites of a regular lattice by collisions. This is a mesoscopic study of the macroscopic problem, which incorporates the basic conservation laws of the hydrodynamic variables such as density and velocity. This scheme is known as the *lattice Boltzmann model* (LBM), initially developed from its predecessor, the *lattice gas automata* (LGA).

The LBM has rapidly evolved into a self-standing research subject and has proved to be an efficient tool for simulating a variety of nontrivial fluid dynamic phenomena. This kinetic description of the fluid motion, based on the Boltzmann equation, is a bridge between a complete molecular description and the real macroscopic world.

The major advantages of the LBM are:

- its explicit feature of the governing equation;
- its intrinsic parallelism;
- its easy numerical implementation, which result into short and fast numerical codes.

LBM is a model able to simulate a few difficult situations, but it is inappropriate in the simulations that consider, for example, high Reynolds and Mach numbers flows. Furthermore, the standard LBM finds severe difficulties in near-grid scale dynamics, which is mostly due to the lack of the H-theorem. The non adherence with the second principle of the thermodynamic often gives very disruptive non-linear instabilities (cfr. Succi in [4]). An approach to overcome these just mentioned problems is a minimal kinetic method based on the Boltzmann equations for hydrodynamics, that is sufficient to give a description of the molecular hydrodynamic motion at a desired length scale. The goal of this approach, recently proposed by Karlin et al. in [5], [6], [7], [8], is the construction of such a scheme that:

- satisfies the H -theorem, which is relevant to the description of the dynamic under consideration;
- shows a higher non-linear stability, which is a desired properties in any numerical scheme.

The aims of this work are:

- the construction of the aforementioned minimal kinetic model for hydrodynamics;
- provide a detailed report on the performance and the accuracy of the minimal models and to compare it with other data available in literature (cfr. Erturk et al. in [9], Hou et al. in [10] and Chen et al. in [11]);
- improve the computational performance of the minimal kinetic model using some numerical optimization strategies;

2. Background

In this section the lattice Boltzmann equation (LBE hereafter) is described. The presentation and the description of the Lattice Boltzmann Model (LBM) could follow different channels (or: at least two channels):

1. through an historical route, that describe the LBM as an evolution of the initial idea of Frisch, Hasslacher and Pomeau in 1986 (cfr. [18]);
2. or through a self-standing research, as proposed and argued by Benzi et al. in [8].

Here we give a short description of the evolution of the model giving the fundamental steps related with the problems and the motivations that brought to a new and advanced formulation of the model that is generated in order to cure the main diseases (as suggested by Succi in [37]).

2.1. Outline of the model history

The fact that different microscopic interactions can lead to the same form of the macroscopic equations, i.e. the Navier-Stokes and the continuity equations, is the starting point for the development of some kind of microscopic methods, as the set of Lattice Gas Cellular Automata (LGCA for short) models. In addition, in considering real gases or liquids (fluids in general), the real world may be seen as interactions of particles that live on a discrete and fictitious world/space and interact each other, obeying the conservation laws of mass and momentum. This kind of models for fluid dynamic base their discrete representation and simulation of the reality on some simple, real and practical laws that lead to an easy representation of the fluid particles (seen as discrete ones). Hereafter a short historical description and evolution of this microscopical model is given, starting from the set of LGCA method till the actual and most used LBGK scheme.

2.1.1. Lattice gas cellular automata

The FHP^a was introduced by Frisch, Hasslacher and Pomeau in 1986 (cfr. [3]) and it is a minimal model for a two-dimensional fluid.

It can be seen as an abstraction, at a microscopic scale, of a fluid.

The FHP model describes the motion of particles traveling in a discrete space and colliding with each other.

The microdynamic of FHP is given in terms of boolean variables describing the occupation numbers n_i at each site of the lattice and at each time step (i.e. the presence $n_i = 1$ or the absence $n_i = 0$ of a fluid particle).

The FHP particles move on a discrete domain, with a six velocity grid shown in Figure 1, with a discrete time step δ_t , a fixed and constant velocity along the links of the computational grid. The dynamics is such that each particle can live and point on each of the six directions of the lattice site, \mathbf{c}_i , $i = 1, \dots, 6$ and no more than one particle can enter the same site at the same computational time.

The dynamic and the evolution of the system is given by the composition of two fundamental phases, i.e. the streaming of the particles along the grid's links, to move from a site to the neighbor, and the redistribution of all the particles arriving at each site.

The particles on the lattice are updated according to a time evolution operator \mathcal{E} which can be described as a convolution:

$$\mathcal{E} = \mathcal{S} \circ \mathcal{C},$$

where \mathcal{C} describe the redistribution and \mathcal{S} the streaming operator.

The full micro-dynamics of the FHP model can be expressed by evolution equations for the *occupation numbers*, $n_i(\mathbf{x}, t)$, defined as the number of particle entering site \mathbf{x} at time t with a velocity pointing along direction \mathbf{c}_i , $i = 1, \dots, 6$, that labels the six lattice directions.

Without interactions between particles, the evolution equations for each n_i sitting at lattice site

^aThe name of the scheme comes from the initial of the three authors.

\mathbf{x} at time t would be given by:

$$n_i(\mathbf{x} + \mathbf{c}_i \cdot \delta_t, t + \delta_t) = n_i(\mathbf{x}, t), \quad (1)$$

which express that a particle entering site \mathbf{x} with velocity along \mathbf{c}_i will continue in a straight line so that, at next time step $(t + \delta_t)$, it will enter site $\mathbf{x} + \mathbf{c}_i \cdot \delta_t$ with the same direction of motion.

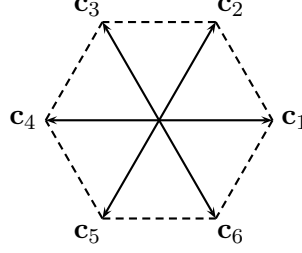


Figure 1. Example of hexagonal and regular lattice.

Equation (1) defines the discrete operator Δ_i as

$$\Delta_i n_i \equiv n_i(\mathbf{x} + \mathbf{c}_i \cdot \delta_t, t + \delta_t) - n_i(\mathbf{x}, t), \quad (2)$$

that can assume only three states:

$$\Delta_i n_i = \begin{cases} 1, & \text{if a particle is added to link } \mathbf{e}_i \\ 0, & \text{if there are no changes to link } \mathbf{e}_i \\ -1, & \text{if a particle is removed from link } \mathbf{e}_i \end{cases} \quad (3)$$

Due to collisions, a particle can be removed from its original direction or another one can be deflected into direction \mathbf{c}_i using statistical rules or probability theories (as shown on image 2).

This formulation let us to simulate the fluid motion and to compute the associated macroscopic variables, i.e. the fluid density ρ and the local fluid velocity \mathbf{u} , by the *occupation number* as:

$$\begin{aligned} \rho &= \sum_{i=1}^b n_i, \\ \rho \mathbf{u} &= \sum_{i=1}^b n_i \mathbf{c}_i. \end{aligned} \quad (4)$$

We conclude this short description of FHP by noticing that this kind of collision rules satisfies two crucial and important properties:

- they conserve the number of particles in each site, i.e. the mass conservation, that can be expressed as:

$$\sum_i n_i(t + 1, \mathbf{x} + \mathbf{c}_i) = \sum_i n_i(t, \mathbf{x}), \quad (5)$$

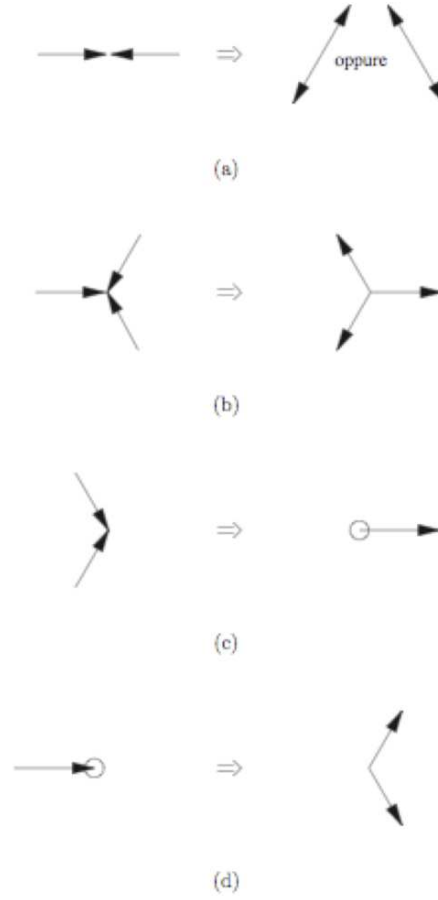


Figure 2. Collision on the FHP model.

- they conserve the total momentum, that is:

$$\sum_i \mathbf{c}_i n_i(t+1, \mathbf{x} + \mathbf{c}_i) = \sum_i \mathbf{c}_i n_i(t, \mathbf{x}). \quad (6)$$

2.1.2. *Micro-dynamical equations and macroscopic quantities*

The macroscopic quantities, reconstructed from the microscopic state by mean of (4), are very noisy since we deal with boolean variables. Furthermore all the physical quantities of interest are not boolean values.

In practice, it is more convenient to average over a small region of the computational domain and of the grid.

Towards this direction Frisch et al. in [12] propose to use a probabilistic approach, which is

traditional in statistical mechanics: they consider the mean population

$$N_i(\mathbf{x}, t) = \langle n_i(\mathbf{x}, t) \rangle, \quad (7)$$

where $\langle \cdot \rangle$ is a proper/appropriate average over the boolean occupation number or over some grid sites.

Thus, according to the rules 1, the microdynamics of a LGCA can be written as

$$N_i(\mathbf{x} + \mathbf{c}_i \cdot \delta_t, t + \delta_t) = N_i(\mathbf{x}, t) + \Omega_i. \quad (8)$$

These quantities are defined from the average $N_i(\mathbf{x}, t) = \langle n_i(\mathbf{x}, t) \rangle$ of the microscopic occupation variables.

Note that $N_i(\mathbf{x}, t)$ is also the probability of having a particle entering the site \mathbf{x} , at time t , with velocity

$$\mathbf{v}_i = \frac{\delta_s}{\delta_t} \mathbf{c}_i. \quad (9)$$

Furthermore, in equation (8), the term Ω_i is the averaged free streaming operator that can be computed using the average function $\langle \cdot \rangle$ and the definition in equation (2), obtaining

$$\Omega_i(n) = \langle \Delta_i n_i \rangle. \quad (10)$$

In general this formulation introduces a strong and sharp change in the treatment and in the consideration of the particle on the lattice site.

Once all the averaged populations were defined, the computation of the macroscopic quantities may be obtained from the combination of equations (7) and (4).

That is the *mean density* is given by:

$$\rho(\mathbf{x}, t) = \sum_{i=1}^b N_i(\mathbf{x}, t), \quad (11)$$

while the *mean momentum* is computed by

$$\mathbf{J}(\mathbf{x}, t) = \sum_{i=1}^b \mathbf{c}_i N_i(\mathbf{x}, t), \quad (12)$$

and, finally, the *mean velocity* may be computed by

$$\mathbf{u}(\mathbf{x}, t) = \frac{\mathbf{J}(\mathbf{x}, t)}{\rho(\mathbf{x}, t)}. \quad (13)$$

2.1.3. Remarks

The conservation laws: It may be underlined that equations (8) and (10) represent the microdynamic equation for the Boolean lattice gas and are the starting point of the analysis that ends up with the Navier-Stokes equations.

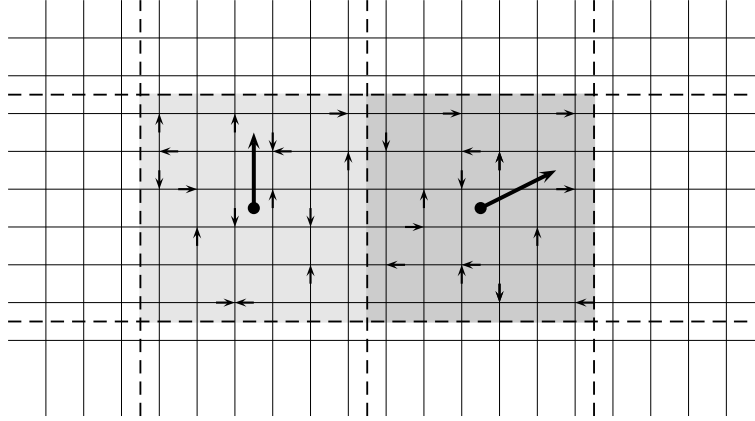


Figure 3. An example of domain of averaging on a section of square lattice with two cells, composed by a average of 6×6 (only for the sake of clarity in the visualization) computational nodes. The two cells, superimposed over the computational grid, are shown and marked by the dashed lines and by the colored zones. The individual particles are represented by the small arrows and the average velocities by the large arrows.

It has to be remarked that, in spite of the drastic reduction of microscopic degree of freedom, the results of the multi-scale analysis can be made basically to coincide with the continuum equations.

It means that, the microscopic procedure respect the fundamental conservation laws of classical mechanics ([12]), which in terms of the model variables can be described as follows:

- Mass and momentum conservation:

$$\sum_i C_i = 0 \quad (14)$$

$$\sum_i c_{i\alpha} C_i = 0 \quad (15)$$

- Angular momentum conservation (rotational invariance).

From LCGA to Navier-Stokes: The standard bottom-up procedure^b proceeds through the following three formal steps:

- From Newton-Hamilton to Liouville
- From Liouville to Boltzmann
- From Boltzmann to Navier-Stokes

^bBy bottom we mean the microscopic level, the idea is that upper levels 'emerge' to the status of macroscopic observables from coarse-graining of the lower levels.

2.1.4. The lattice Boltzmann models

In spite of all the interesting results, LGCA appeared to be inadequate in the fluid-dynamic simulation controlled by the Navier-Stokes equation. Indeed they are plagued by several diseases (cfr. [4]) and the most relevant are:

Violation of the galilean invariance: the lack of galilean invariance appears in dealing with the density of particles ρ “living” on each grid site that have to run on a constant density. Some of the troubles deriving from this pathology have been studied by Gunstensen et al. in [13] and by d’Humières et al. in [14], using different strategies.

Anomalies: Anomalous and explicit dependence of the pressure on the velocity vector, which is related to the grid construction (cfr. [4]).

Statistical noise: one major draw-back of LCGA is the statistical noise in the computed hydrodynamic fields. This is a direct consequence of the single particle boolean operation: one method to smooth out the noise is to average in space and time, which, however, limits the space resolution that can be chosen. Another way is by replace the boolean variables with real-valued densities of microscopic particles.

Enormous memory and computational demand: it is easy to see that in the microdynamic of LCGA simulation good results need $O(2^b)$ boolean operations, in dealing with a b -bit automaton. It means that in 2D simulations ($b = 6$) the computational demand is admissible, but in 3D simulations ($b = 24$) the cost is prohibitive.

Spurious invariants: are pure artifact that produce some unwanted effects and unphysical conserved quantities (as, for example, lack of ergodicity, the system dynamics is over-constrained).

For most of them, as we are going to see, the introduction of a Boltzmann based theory is a therapy.

The next sections are devoted to the description of the so called lattice Boltzmann models (LBM).

The LBM may be seen as an evolution of the lattice gas models (LGCA), which try to overcome the main problems, especially the statistical noise. Our description of the model starts with the nonlinear lattice Boltzmann equation (LBE for short), used to approach the complete and modern version of the lattice Boltzmann model (LBM).

The new scheme starts from the idea, firstly proposed by McNamara and Zanetti in 1988 (cfr. [15]), to replace the boolean occupation number n_i , with averaged populations:

$$f_i = \langle n_i \rangle, \quad (16)$$

where $\langle \cdot \rangle$ stands for an appropriate average.

The averaged quantities $f_i = f_i(\mathbf{x}, t)$ are now real function ranging between 0 and 1, depending on the site \mathbf{x} and on time t .

As for the boolean variables n_i , the computation of the associated macroscopic variables can be done using the sum on the links of the grid, as described by equations (4), but considering

the populations f_i in spite of the boolean occupation numbers n_i .

The evolution of the distribution function $\mathbf{f} = (f_1, \dots, f_b)$ is found by the collision operator using the following rule:

$$f_i(\mathbf{x} + \mathbf{c}_i, t + \delta_t) - f_i(\mathbf{x}, t) = \Omega_i(\mathbf{f})\delta_t, \quad (17)$$

where the collision operator $\Omega_i(\mathbf{f})$ is the local average on the lattice gas collision operator $\langle \Omega_i(n) \rangle$, defined in equation (7), as follows:

$$\Omega_i(\mathbf{f}) = \langle \Omega_i(n) \rangle. \quad (18)$$

The collision operator is one of the crucial step in the evolution of the LBM. One of the first and main formulation was the *quasi linear* collision operator, proposed by Higuera and Jimenez in [16]:

$$\Omega_i(\mathbf{f}) = A_{ij}(\mathbf{f}_j - \mathbf{f}_j^{eq}), \quad (19)$$

where A_{ij} is the scattering matrix, that can be computed directly from the transition matrix (for detail see [4]).

We can remark that the negative-definiteness property of the matrix A_{ij} ensures the compliance with the H -theorem, i.e. the fulfilment of the second principle of thermodynamic^c. A few properties of the scattering matrix lead to the evolution of a new collision operator for the evolution of the fluid system, which reduce the complex and large scattering matrix with a single time relaxation operator.

This new approach was developed especially after the introduction of the celebrated BGK method^d (cfr. [17]).

All the other eigenvalues in the scattering matrix A_{ij} control the interference of non-hydrodynamic modes with the dynamic of the macroscopic variables.

This observation (Chen et al in [18], Koelman in [19] and Qian et al. in [20]) gave rise to the idea of a diagonal scattering matrix with the unique eigenvalue ω , on the diagonal, that control the viscosity value. The scattering matrix is replaced by its diagonal form

$$A_{ij} \hookrightarrow -\omega\delta_{ij}, \quad (20)$$

where ω is the relaxation frequency toward the local equilibrium.

It may be observed that:

- the relaxation frequency is limited, i.e. $\omega \in (0, 2)$, for the sake of numerical stability;
- the relaxation frequency ω is related to the kinematic viscosity ν of the fluid by the following relation:

$$\nu = \frac{c^2}{3} \left(\omega - \frac{1}{2} \right) \quad \Rightarrow \quad \omega = \left(\frac{1}{2} - \frac{3}{c^2} \nu \right), \quad (21)$$

where $c = \delta_x/\delta_t$ is the grid velocity.

Equation (21) let us understand that the value of the relaxation parameter has a constant value for all the simulations in the LBGK model.

^cAs we will see, the accordance with the H -theorem is a non-trivial question.

^dBGK derives from the names of the three authors Bhatnagar-Gross-Krook

In this way, moving from a multi relaxation (one for each macroscopic variable that play a role in the fluid-dynamic phenomenon) to a single relaxation time model, we obtain the lattice Bhatnagar-Gross-Krook (LBGK for short) model, described by

$$\Omega_i(\mathbf{f}) = -\omega(f_i - f_i^{eq}). \quad (22)$$

This formulation for the update gives a simple, easy to use and computational-saving model, that we are going to describe in next section.

The complete LBGK scheme is obtained reminding equation (17), that describes and controls the evolution of the system, and coupling it with the LBGK equation, used in the updating step.

For the sake of clarity, the complete equation is:

$$f_i(\mathbf{x} + \mathbf{c}_i, t + \delta t) - f_i(\mathbf{x}, t) = -\omega(f_i - f_i^{eq}), \quad (23)$$

with $f_i(\mathbf{x}, t) \equiv f(\mathbf{x}, \mathbf{v} = \mathbf{c}_i, t)$ representing the probability of finding a particle at lattice site \mathbf{x} at time t , moving along the lattice direction defined by the discrete speed \mathbf{c}_i .

Remark 1. It is important to underline that all the considerable advantages, from the computational and from the implementation point of view, brought by the LBGK approximation are not free of costs.

Indeed in previous section, we listed all the properties of the scattering matrix, especially the negative-definiteness that is the basic assumption for the compliance with the second principle of the thermodynamic.

The price is the loss of the linear stability and with it the second principle of the thermodynamic (i.e. the H -theorem).

Our starting point is the LBGK equation (23) describing the time evolution of a set of a discrete population of particles $\mathbf{f} = (f_0, \dots, f_{b-1}) \in R^b$.

The left-hand side of equation (23) represents the molecular free-streaming, whereas the right-hand side represents molecular collisions via a single-time relaxation towards local equilibrium f_i^{eq} on a typical single timescale ω . The parameter ω is the relaxation rate, characterized by a non-linear dependency on δt (as derived by S. Ansumali in [5]).

The local equilibrium \mathbf{f}_i^{eq} is taken in the form of a quadratic expansion of a (local) Maxwellian:

$$f_i^{eq} = \rho w_i \left[1 + \beta u_i + \frac{\beta^2}{2} (u_i^2 - u^2) \right], \quad (24)$$

where w_i are weighting factors related to the computational grid, $u_i = \mathbf{u} \cdot \mathbf{c}_i$, $\beta = 1/c_s^2$ and c_s being the lattice sound speed, defined by the equation $c_s^2 = \sum_i w_i (\mathbf{c}_i \cdot \mathbf{c}_i)$.

The value of all the just mentioned parameters depends on the grid, the usual ones are listed in Table 1. In the isothermal case, which we are interested in, local hydrodynamic variables are

Name	c_s^2	Grid Weight w_i
D1Q3	1/3	4/6 1/6
D2Q9	1/3	16/36 4/36 1/36
D3Q15	1/3	16/72 8/72 1/72
D3Q19	1/3	12/36 2/36 1/36

given by

$$\rho = \sum_i f_i, \text{ fluid density,} \quad (25)$$

$$\mathbf{u} = \frac{\sum_i \mathbf{c}_i f_i}{\rho}, \text{ flow velocity.} \quad (26)$$

This procedure, in the limit of small oscillations from local equilibrium, i.e. small Knudsen numbers [4], leads to the real phenomenon and it has been shown that the Navier Stokes equations may be obtained from the Boltzmann equation by the Chapman Enskog procedure under constraints of isotropy and Galilean invariance only on the equilibrium distribution (as shown by Love et al. in [21]). The mentioned procedure requires that the set of discrete speeds satisfy mass, momentum and energy conservation laws, as well as rotational symmetry. It is straightforward to convince that this derives by imposing the following constraints on the local equilibrium distribution:

$$\begin{aligned} \sum_i f_i^{eq} &= \rho, \\ \sum_i f_i^{eq} \mathbf{c}_i &= \rho \mathbf{u}, \\ \sum_i f_i^{eq} (\mathbf{c}_i \cdot \mathbf{c}_i) &= \rho (\mathbf{u} \cdot \mathbf{u}) + \rho c_s^2 I. \end{aligned}$$

It has to be remarked that discrete Maxwellians, i.e. Maxwellian equilibria with the plain replacement $\mathbf{v} = \mathbf{c}_i$ would not fulfill the conservation constraints for any generic value of the flow speed u . To overcome this difficulty, local Maxwellians have been expanded in powers of the Mach-number, and typically replaced by second (or higher) order polynomials^e.

It has to be remarked that only a limited class of lattices exhibits the right symmetry to ensure

^eIn the entropic method, the approximation of the Maxwellian equilibria is lifted up a fourth-order in the Mach number, by an irrational expressions.

the conservation constraints (a few are listed in Table 1 and showed in Figures 4, 5, 6).

In the present work we shall refer to the bi-dimensional nine-speed lattice (D2Q9) defined as:

$$c_i = \begin{cases} 0, & i = 0, \\ \cos((i-1)\pi/2), & i = 1, \dots, 4, \\ \sqrt{2}\cos(\pi/4 + (i-5)\pi/2), & i = 5, \dots, 8, \end{cases} \quad (27)$$

with weights $w_0 = 4/9$, $w_1 = 1/9$, $w_2 = 1/36$, as listed in Table 1.

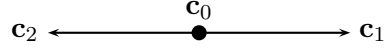


Figure 4. The D1Q3 lattice.

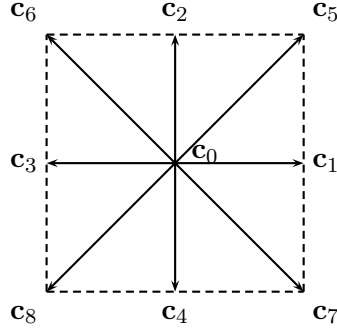


Figure 5. The D2Q9 lattice.

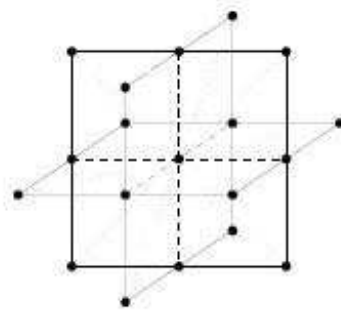


Figure 6. The D3Q19 lattice.

2.1.5. *Remarks*

To conclude the description of the historical evolution of the model, we describe some distinctive features of the LB model versus LGCA:

- the model is suitable and convenient to modern machine for the computation and simulation of fluid-dynamic phenomena;
- it is apt to describe mesoscopic physics and phenomena, that are not so easy to study with a traditional approach.

The attainment of these results is not free of costs. One of the price to pay is that the computational costs together with the round-off errors increase due to the use of floating point variable in spite of a boolean algebra.

2.1.6. *Remarks*

As expected, the linear LBE maintains some good and bad characteristic of its ancestor LGCA.

For example:

- With the LGCA model the 3D simulations are computationally too expensive, and the linear LBE formulation maintains this characteristic (that will be solved by the more accurate non-linear LBE, which will be described later in this article).
- The fact to maintain the micro-dynamic physical phenomena, let us be in compliance with the second principle of thermodynamic. This is an important characteristic of the LGCA that linear LBE has inherited.

3. Entropic models

It is known that the non-positivity of the distribution function causes numerical instabilities in the LB method (see for details [22], [23], [20], [4]). To overcome this problem Karlin et al. in [6, 24, 25, 8, 7, 26] propose a scheme that satisfy the second principle of the thermodynamic by imposing the monotonicity and the minimality of the H -function.

The aforementioned model, is named entropic lattice Boltzmann model (ELBM for short).

ELBM acts on the local equilibrium \mathbf{f}^{eq} because of if the local equilibrium is supported by some entropy function, then the Lattice Boltzmann method can be equipped with the H -theorem, (as refers in [27], [26], [25], [28], [29]) and stability problem can be studied in a controlled way. Before giving more details about the model, let us briefly describe the theoretical motivations.

3.1. *Theoretical motivations*

In considering a system relaxing from the initial non-equilibrium state to the final equilibrium state, it is a common practice to distinguish between three regime (as described by Gorban et al. in [30]):

- the early time relaxation, immediately after the system leaves the initial non-equilibrium state f_0
- the intermediate regime
- the final regression towards the equilibrium state f^0

This picture of the system evolving towards the final equilibrium state is particularly visible in the evolution of gases, where the relaxation process is dominated by the collision integral $Q(f)$ computed at the initial state f_0 . Let

$$Q_0 = Q(f_0) \quad (1)$$

be the well-known collision rate in the phase space function, and

$$f(\Gamma, a) = f_0(\Gamma) + aQ_0(\Gamma) \quad (2)$$

be the necessary step to let the system pass through different states, where $a \geq 0$ is a scalar variable.

This approximation is valid only if a is not too large, that is if a do not exceed a certain limiting value a^* , corresponding to a state f^* that can be represented as

$$f^*(\Gamma) = f(\Gamma, a^*) = f_0(\Gamma) + a^*Q_0(\Gamma). \quad (3)$$

The limit value a^* plays a central role in the definition of ELBM.

Let $S(f)$ be the entropy value of the state $f(\Gamma)$, and let $S(a)$ be its value in the state $f(\Gamma, a)$, derived by eq. (3).

On the base of the Q_0 -dominated dynamics, each state is accessible if and only if the entropy production grows in the interval $[0, a]$. The upper limit $a^* \in [0, a]$ is characterized by the following:

1. the entropy $S(a)$ increase from 0 to a^* ,
2. the entropy $S(a)$ decrease as a overcomes a^* .

Furthermore, $f(\Gamma, a^*)$, with a satisfying the aforementioned properties, is unique.

Assuming that the motion of the system is described by

$$\partial_t f(\Gamma, t) = Q(f), \quad (4)$$

we can state that the entropy increases monotonically along the space of solutions. A standard example of this kind of equation is the Boltzmann equation (that is the basis of the kinetic models we are dealing with).

Furthermore, if $f(\Gamma, a)$ is the solution of equation (4) it satisfies the condition $f(\Gamma, 0) = f_0(\Gamma)$. In this just mentioned case, the phase trajectory of this solution can be represented by the function $f(\Gamma, a)$, with $a \in [0, 1]$. In addition, for each value of the parameter a , the function $f(\Gamma, a)$ assumes a non-negative value as function of Γ , since the entropy is a growing function of $a \in [0, a^*]$. This let us conclude that the Boltzmann equation can be used as the basis of a method for the construction of the trajectory $f(\Gamma, a)$, that is the basis for the lattice Boltzmann model.

3.2. Loss of compliance with the H -theorem

As described in previous chapter, the linear LBGK model brought a lot of improvements in the Boltzmann kinetic scheme.

Indeed the single-time relaxation scheme is a very simple task (from the practical and theoretical point of view) and it is difficult to imagine a simpler model that recover the Navier-Stokes equation. Moreover, it has been already remarked that the diagonal form for the collision operator is supported by the first principle of the thermodynamic, i.e. the conservation laws of the mass and momentum are respected.

Using the LBGK form for the collision operator, the property of non-positiveness of the scattering matrix is lost and with it the compliance with the second principle of thermodynamic. ELBM is a strategy to overcome the lack of the linear stability of the standard LBGK model.

3.3. Construction of the entropic model

The lack of compliance with the H -theorem is a problem whose effects have been felt throughout many authors (cfr. [4]). For this reason the construction of a method that recover the physical connection to this theorem and, with it, the linear stability, could be very interesting and able to give more truthful simulations.

Progress on this direction have been achieved by a class of lattice Boltzmann models known as entropic lattice Boltzmann models (ELBM), developed during the last decade by Karlin et al. (cfr. [5], [24], [6], [7], [8]).

ELBM (cfr. [8], [25]) attempts to enhance stability via an H -theorem, through entropy functions whose local equilibria are suitable to recover the Navier-Stokes equations.

The novelty of ELBM is principally represented by two features:

- the definition of the local equilibrium distribution function as the minimizer of the H -function;
- the computation of the relaxation parameter in order to satisfy the local monotonicity of the H -function.

Let us describe this innovation introduced by ELBM, in the following sections.

3.3.1. The H -function

In the construction of an H -function for the entropic version of the LBGK, we base on the following important observation:

“If discrete velocities are constructed from the zeros of the Hermite polynomials, the method of discrete velocity is essentially equivalent to Grad’s moment method based on the expansion of the distribution function around a fixed Maxwellian distribution function.”
(as stated by Karlin et al. in [8]).

The natural and simplest way to use this approach in an entropic formulation is to link the discrete Boltzmann model to an entropic Grad’s method (cfr. [31]). We know that the continuous

Boltzmann's H -function is a convex function given by:

$$H = \int F(\mathbf{x}, \mathbf{c}, t) \ln F(\mathbf{x}, \mathbf{c}, t) d\mathbf{c}, \quad (5)$$

where $F(\mathbf{x}, \mathbf{c}, t)$ is the one-particle distribution function, \mathbf{x} the position vector, t the observation time and \mathbf{c} is the continuous velocity vector.

For 1D isothermal flows, a discrete form of the H -function can be directly computed from equation (5). For higher dimension flows a discrete form for the H -function is computed by means of the Gauss-Hermite quadrature formulas (as in [32] and [7]).

Indeed we know that the Hermite coefficients are directly related to the macroscopic fluid variables such as density, velocity, internal energy and stress. Furthermore, there is a direct correspondence between the approximation by Hermite polynomial expansion with the LBE method, and the grid velocity vectors, i.e. the Hermite coefficients (cfr. [32]). So, using the Hermite quadrature formulas we obtain the following discrete expression for the H -function on a DnQm LBM site:

$$H_{(w_i, \mathbf{c}_i)} = \sum_{i=1}^b f_i \ln \left(\frac{f_i}{w_i} \right), \quad (6)$$

where w_i are the weights associated with the i -th particle speed \mathbf{c}_i and b is the total number of links.

Furthermore, in D dimensions, the one-particle distribution function $F(\mathbf{x}, \mathbf{c}, t)$ function is related to the i -th particle distribution function as follows:

$$f_i(\mathbf{x}, t) = w_i (2\pi T_0)^{(D/2)} \exp \left[\frac{\mathbf{c}_i^2}{2T_0} \right] F(\mathbf{x}, \mathbf{c}, t), \quad (7)$$

where T_0 is the reference temperature.

It has to be remarked that if the discrete velocities are formed using roots of the third order Hermite polynomials, the Navier-Stokes equation is reproduced up to the order $O(u^2)$.

3.3.2. The equilibrium distribution function to get the minimum value

It has to be remarked that:

- the functional form of the equilibrium distribution function in the velocity space, is only relevant in computing the low order moments;
- those moments can be computed exactly using a Gaussian quadrature formulas.

The aforementioned remarks, let it follows that the Navier Stokes equation can be derived from the Boltzmann equation by an evaluation of the Hermite quadrature formulas on the nodes.

The expression of the associated equilibrium distribution f_i^{eq} , obtained from solving the minimization problem, has the following form (as in [8]):

$$f_i^{eq} = \rho w_i \prod_{j=1}^D \left(2 - \sqrt{1 + u_j^2} \right) \left(\frac{2u_j + \sqrt{1 + 3u_j^2}}{1 - u_j} \right)^{\mathbf{c}_{ij}/\mathbf{c}}, \quad (8)$$

where j is the index of the spatial directions.

The derivation of the equilibrium (8) is based on the discrete form of the entropy function (6), which is computed using the Hermite quadrature (the polynomial equilibria of the lattice Boltzmann method as in [32]).

3.4. The relaxation parameter

The knowledge of the H -function suggests the realization of an entropic version of the lattice Boltzmann method, i.e. ELBM. In this section, the basic concept and the complete procedure for the realization of the entropic scheme are given.

The monotonicity constraint on the H -function is imposed through a two-steps geometric procedure:

- in the first step, populations are changed in the direction of the bare collision, $\Delta = \mathbf{f}^{eq} - \mathbf{f}$ (as given by Karlin et al. in [24]) such that the H -function remains constant;
- in the second step, dissipation is introduced and the magnitude of the H -function decreases.

Let us explain better the aforementioned procedure.

3.4.1. First step:

To force the monotonicity of the H -function a collision integral $\Delta(\mathbf{f})$ is defined in the kinetic equation, defined as:

$$\Delta(\mathbf{f}) = \mathbf{f}^{eq} - \mathbf{f}. \quad (9)$$

$\Delta(\mathbf{f})$ is said “admissible” if it satisfies the following two conditions:

- the conservations laws of mass and momentum;
- the entropy production inequality

$$\langle \nabla H | \Delta \rangle \leq 0, \quad (10)$$

where $\nabla H = \{\partial H / \partial x_i\}_{i=1, \dots, D}$ is the gradient of the entropy function, which gives ($\mathbf{f} = \mathbf{f}^{eq}$) if the equality holds in equation (10).

Remark 2. The standard BGK collision integral, for instance, is admissible.

$\Delta \mathbf{f}$ is used to obtain a constant value for the entropy production at each time step. To have the just mentioned condition let us introduce an auxiliary population

$$\mathbf{f}^* = \mathbf{f}_{\alpha^*} = \mathbf{f} + \alpha^* \Delta \quad (11)$$

where the scalar parameter α^* , that is the upper limit for the updating rule, is the solution of the following equation:

$$H(\mathbf{f}) = H(\mathbf{f} + \alpha \Delta). \quad (12)$$

A geometric interpretation of equation (12) in the phase space (described in figure 1), let us characterize its solutions as follows:

- $\alpha_1 = 0$
- α_2 can assume the following values:
 - the *degenerate case* $\alpha_2 = \alpha_1 = 0$, that occurs only if $\mathbf{f} = \mathbf{f}^{eq}$;
 - the *boundary case*, where

$$\alpha_2 = \alpha^* = \min_{i=0,\dots,b-1; \Delta_i < 0} \left\{ \frac{\mathbf{f}_i}{|\Delta_i|} \right\}. \quad (13)$$

Here the auxiliary population, that fixes the limit of the collision operator in the update step, is taken at the boundary of the phase space;

- the *standard case*, where α_2 is computed numerically from equation (12) by a root finder.

3.4.2. Second step:

Once the auxiliary population \mathbf{f}^* has been defined, the collision is set as:

$$\mathbf{f}(\beta) = (1 - \beta)\mathbf{f} + \beta\mathbf{f}^*, \quad (14)$$

where $\beta \in [0, 1]$ is a fixed parameter that controls the viscosity coefficient in the Navier-Stokes equation.

The computation of the viscosity coefficient and of the parameter β , related to it, is realized on the basis of the Chapman-Enskog analysis in the vicinity of the local equilibrium. This just mentioned computation is the same way as in the standard lattice Boltzmann scheme (for further details see [24]), i.e. it is given by:

$$\nu = c_s^2 \left(\frac{1}{\alpha\beta} - \frac{1}{2} \right) \delta t, \quad (15)$$

where $\nu_0 = \nu$ is the fluid kinematic viscosity that acts on the model by the parameter β , that can be obtained by some algebra from equation (15):

$$\beta = c_s^2 \frac{\delta t}{2\nu_0 + \delta t}, \quad (16)$$

where c_s is the already mentioned sound speed.

The two steps scheme just described gives the ELBM and is able to retain the full control over the viscosity.

3.5. Theoretical remarks on the progression of the H -function

In this section some remarks about the value of the parameter α are given. The updating rule on the entropic model is based on a scheme where the monotonicity of the H -function is prescribed by the simple rule described in section 3.3.1.

The solution of equation (12) assume a few crucial and remarkable values. Let us explain better.

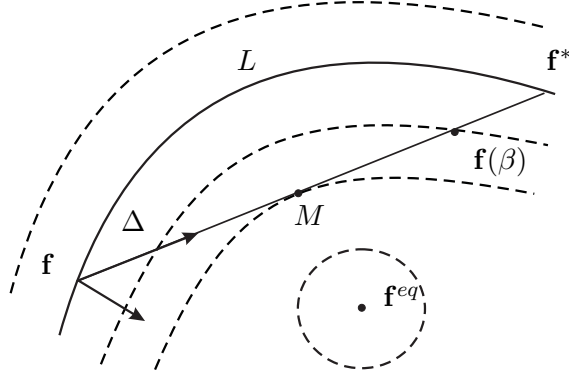


Figure 1. Stabilization procedure in the phase space. The dashed curves represent the entropy levels surrounding the local equilibrium \mathbf{f}^{eq} . The solid curve L is the entropy level at a fixed time step with the value $H(\mathbf{f}) = H(\mathbf{f}^*)$, where \mathbf{f} is the initial while \mathbf{f}^* is the auxiliary population. The vector Δ is the bare collision integral and M is the point where the local entropy production is minimal. The result of the collision update is given by the value $\mathbf{f}(\beta)$, that represent a point of *over-relaxation*, i.e. $H(\mathbf{f}(\beta)) > H(M)$, but the entropy production decrease, i.e. $H(\mathbf{f}(\beta)) < H(\mathbf{f}^*)$, and the conditions of the H -theorem are fulfilled.

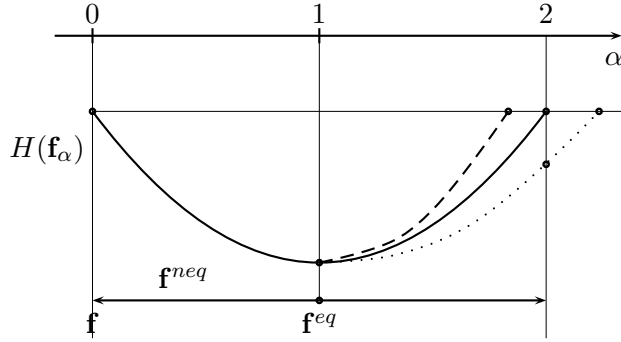


Figure 2. Local evolution/progress of the H -function around the equilibrium distribution function \mathbf{f}^{eq} . The continuum curve plots a local quadratic/parabolic H -function, while the dashed and dotted curves plots an H -function corresponding to a locally under and over relaxed system, respectively.

The population \mathbf{f}_α can be expressed in a simplified way around the local minimum of the H -function:

$$\begin{aligned} \mathbf{f}_\alpha &= \mathbf{f} + \alpha \Delta \\ &= \mathbf{f} + \alpha(\mathbf{f}^{eq} - \mathbf{f}) \\ &= (1 - \alpha) \cdot \mathbf{f} + \alpha \mathbf{f}^{eq}, \end{aligned} \tag{17}$$

where \mathbf{f} is the population before the collision step and \mathbf{f}_α is the population defined in equation (11).

A deep study of equation (17) and the geometrical interpretation of the monotonicity of the H -function around its local minimum (schematized in figure 1), give the following two remarks:

- the old population \mathbf{f} limits from below the new value;
- the equilibrium distribution function \mathbf{f}^{eq} fix a central value for α ;

The lower and upper bounds, given for the populations, are associated to a value of the parameter α , i.e. $\alpha = 0$ and $\alpha = 1$ respectively, which implies that $\alpha \in [0, a]$ with $a > 1$. Furthermore we can observe that:

Case $\alpha = 0$: corresponds to a static situation, that is, replacing in eq. (17) the value $\alpha = 0$ we obtain:

$$\mathbf{f}_\alpha = \mathbf{f}; \quad (18)$$

Case $\alpha = 1$: corresponds to a population equal to the equilibrium population \mathbf{f}^{eq} , which let achieve the local minimum value for the H -function.

Replacing in equation (17) the value $\alpha = 1$, indeed, we obtain:

$$\mathbf{f}_\alpha = \mathbf{f}^{eq}; \quad (19)$$

Case $\alpha \in (0, 1)$: the H -function is a monotonic decreasing function;

Case $\alpha = 2$: corresponds to a special solution of equation (12) that gives the following value for the population \mathbf{f}_α :

$$\mathbf{f}_\alpha = \mathbf{f}^{eq} - \mathbf{f}^{neq} > 0 \quad \text{if} \quad \mathbf{f}^{neq} < \mathbf{f}^{eq}; \quad (20)$$

Case $\alpha \in (1, 2)$: the H -function is a monotonic increasing function.

In addition for each value of $\alpha \in [0, a]$ we have a different progression of the H -function, i.e.:

1. If H is locally a quadratic function around the local equilibrium and the value $\alpha = 1$ corresponds to the abscissa of the vertex of this parabola. This case is plotted in figure 2 by the continuum line.
2. If H is not locally a parabolic function, the solution of equation (12) may be < 2 or > 2 , which match to an under and over relaxation of the scheme, respectively. These cases are geometrically described in Figure 2, where the dashed lines describe a possible H -function with an under relaxation solution, while the dotted line correspond to an H -function describing an over relaxed local evolution.

These are all the possible configuration for the H -function around the local minimum value during the evolution process.

3.5.1. ELBM updating rule

In previous sections the numerical procedures to compute a relaxation parameter that limit the variation of the H -function was given. In addition it was defined an equilibrium distribution function that maximize the entropy production (cfr. equation (8)).

To have the complete description of the entropic scheme we need a suitable updating rule, that combines these two parts.

Remarking that the entropic lattice Boltzmann method is build along the lines of the LBGK, the rule for the update follows the usual scheme:

$$f_i(\mathbf{x} + \mathbf{c}_i \delta t, t + \delta t) = f_i(\mathbf{x}, t) + \theta (f_i^{eq} - f_i), \quad i = 0, \dots, b-1, \quad (21)$$

where:

- the *effective* relaxation frequency

$$\theta = \alpha \cdot \beta, \quad (22)$$

is delivered by the geometrical procedures described in section 3.4.1;

- the equilibrium distribution function f_i^{eq} , as computed in section 3.3.2.

In this way the scheme satisfies the second principle of thermodynamic and the monotonicity of the H -function.

3.6. Numerical applications

A number of numerical tests have demonstrated the unconditional stability of the lattice Boltzmann models equipped with the H -theorem (cfr. [24] – [27], [33], [34], [35]), as described previously.

Here we address the accuracy and the performance of the ELBM with respect to the lattice LBGK scheme by a standard benchmark problem, i.e. the lid driven cavity flow; and we study and describe some optimization strategies used in order to reduce the computational cost of ELBM. These strategies are proposed and numerically demonstrated.

3.7. Description of the problem

In this chapter we show the benefits that ELBM brings to a fluid dynamic Lattice Boltzmann simulation.

The benchmark test used to address and to test the accuracy of the ELB method and to compare it with standard LBGK and literature data, is the lid-driven Cavity Flow. This is a

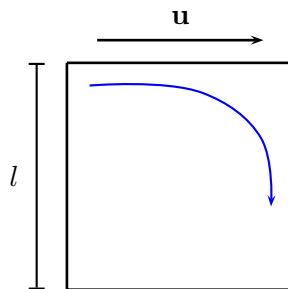


Figure 3. Computational domain: lid driven cavity flow.

steady, incompressible flow that sets up in a square box with wall boundaries, where one of the

walls (here the top one) moves at a constant velocity \mathbf{u} (as shown in Figure 3).

Despite its simple geometry, a complex flow takes place into the square cavity, with multiple counter-rotating recirculating regions.

When in the simulation we reach the steady state, three main vortices of different dimensions are usually observed, coupled with some little ones:

- a pair of small vortices (left and right secondary vortices) is located in the lower corners;
- a big vortex occupies the upper portion of the cavity (primary vortex);
- fourth vortex at the bottom left corner is observed for $Re \geq 5000$, as found by Karlin et al. in [6].

3.8. Numerical settings for the simulations

Once the viscosity value, the shape and the dimensions of the cavity are fixed (as in Fig. 3), the complexity of the flow depends only on the value of the Reynolds number, computed in terms of the cavity width (L) and of the plate speed (\mathbf{U}) as:

$$Re = \frac{L\mathbf{U}}{\nu}. \quad (23)$$

In our simulation and settings, the length of the cavity is $L = l$ (as in Figure 3) and the velocity of the upper boundary is $\mathbf{U} = \mathbf{u}$.

This flow problem has been studied extensively in the numerical literature, therefore accurate results are available for comparison (cfr. Erturk et al. in [9] and Hou et al. in [10]).

In order to evaluate the accuracy of entropic model we use the following settings for the simulations:

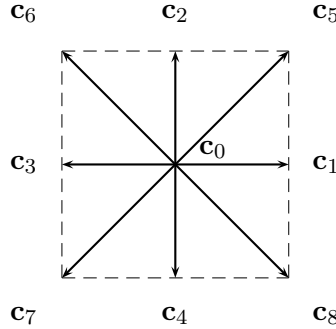


Figure 4. Bi-dimensional grid with nine velocity speed vectors, referred as D2Q9.

- the top boundary moves from left to right with a constant and uniform velocity $\mathbf{u} = (0.1, 0)$, in lattice units;
- the computational domain is discretized with 100×100 nodes along the two cartesian coordinates. The bi-dimensional $D2Q9$ lattice was used for the simulation (as shown in Figure 4);

- a uniform initial density $\rho = 2.7$ is set;
- the initial fluid velocity field is set to zero everywhere, except at the top-side nodes, in order to start the evolution of the fluid phenomenon.

The tests were performed using both standard LBGK and ELB model with different values of the Reynolds number, ranging between 400 and 7500. All these cases were made to compare the qualitative data with the standard model and with the literature results, and to study accurately all the advantages, if they exist, of the entropic version of the lattice Boltzmann model.

Before looking at the numerical results, it must be mentioned that, with a coarse 100×100 grid^f, we have:

- the standard LBGK model gives reasonable results only in all the simulations that use a Reynolds number Re up to 2000;
- the ELB method allowed to reach $Re = 7500$, using the same computational grid size.

This remark allow us to state that the Boltzmann model equipped by the H -theorem, i.e. ELBM, could be pushed to higher Reynolds numbers for the enhancement in the stability during the simulation (as we are going to show in the following paragraphs).

3.8.1. *Vortices position*

The quantitative result usually taken as a reliable indicator of accuracy in a simulation on a cavity is the location of the primary and secondary vortices center. Using these just mentioned data, the comparison with literature results is an easy task and a robust indicator of accuracy. As summarized in table ??, we conclude that the data obtained by ELBM are comparable with literature.

In the aforementioned table, all the coordinates of the vortex centers (in particular of the primary, the lower left and right vortex) show that ELBM is able to obtain data comparable and very close to the ones obtained via the standard lattice Boltzmann method (for Reynolds up to 2000, where the data computed with LBGK are reliable) and with the ones given by Hou et al. in [10].

The table shows an excellent agreement between them.

3.8.2. *Stream function*

To visualize all the vortices that are produced and their evolution on the cavity, we can use the stream function value.

The distribution of this function is a very good instrument to give a qualitative study of the phenomenon.

Figures 5 (a), 5 (b), 6 and 7 compare the steady stream function distribution in the cavity, obtained with LBGK and ELB. The plots highlight the existence of a primary and two secondary

^f A 100×100 grid size was used just for computational reasons.

Re		Primary vortex		Lower left vortex		Lower right vortex	
		x	y	x	y	x	y
400	a	0.5608	0.6078	0.0549	0.0510	0.8902	0.1255
	b	0.5500	0.6000	0.0500	0.0500	0.8850	0.1250
	c	0.5500	0.6070	0.0450	0.0600	0.8950	0.1400
1000	a	0.5333	0.5647	0.0902	0.0784	0.8667	0.8667
	b	0.5260	0.5620	0.0900	0.0770	0.8550	0.1150
	c	0.5230	0.5550	0.0900	0.0800	0.8400	0.1000
2000	a	0.5255	0.5490	0.0902	0.1059	0.8471	0.0980
	b	0.5200	0.5500	0.0890	0.1000	0.8300	0.1000
	c	0.5200	0.5540	0.0900	0.1100	0.8350	0.1000
5000	a	0.5176	0.5373	0.0784	0.1373	0.8078	0.0745
	b	0.5150	0.5400	0.0780	0.1350	0.8050	0.0750
7500	a	0.5176	0.5333	0.0706	0.1529	0.7922	0.0667
	b	0.5100	0.5350	0.0700	0.1500	0.7900	0.0700

vortices and show their position in the cavity.

A more accurate study of the pictures let us realize the following observations:

- the differences between LBGK and its entropic version (ELB) is not significant for $Re = 400$ and for $Re = 1000$;
- at $Re = 2000$, we can observe a situation where different nodes are not “synchronized” (because α is not 2).

At the same value for Reynolds number, the streamlines computed with the LBGK method show that some wiggles start to appear, which anticipate loss of numerical stability of the standard LBGK model;

- only with the entropic model we were able to simulate the cavity flow problem at $Re > 2000$.
- the LBGK model is high instable and not able to reach reliable results.
- due to the coarse grid used (100×100), the shape of this vortex is highly distorted, but visible nonetheless.
- the large-scale vortices are well resolved, in spite of the grid coarseness.

We underline that when one draws stream function, they look poor also by the graphical software used. Velocity field is a better indicator.

3.8.3. Velocity profiles

In this section a quantitative evaluation of the entropic model is given via the transverse and the longitudinal velocity profiles, x - and y -components, at the centreline $x = L/2$, where L is

the length of the square domain side.

In order to evaluate the velocity profiles, they are plotted in Fig. 8, for three different Reynolds numbers, that is for $Re = (400, 1000, 2000)$. Figures show an excellent agreement between the results obtained with the simulations based on the entropic version of lattice Boltzmann model, ELBM, and literature data (cfr. Erturk et al. in [9]). It can be appreciated for all three values of the Reynolds number in the pictures 8 (a) and 8 (b).

4. Error analysis: effect of lattice size

In this section the effect of the lattice size on the accuracy of the numerical solution, given by the entropic lattice Boltzmann model, is investigated. To this purpose, the flow simulation on the cavity, described in previous sections, was repeated using four different grid sizes $N \times N$ for the computational domain.

In details, we take $N \times N$ equal to: 50×50 , 100×100 , 200×200 and 500×500 .

As in the simulations described previously, we assumed that the top wall velocity was fixed at 0.1, in lattice units. Furthermore, a Reynolds number $Re = 1000$ was considered, in order to ensure reliable results for all the computational grid used in this case.

The grid effect is measured according to the relative velocity errors proposed by Higuera et al. in [10]:

Lattice size		50×50	100×100	200×200
E_1	(a)	0.28291	0.12227	0.02880
	(b)	0.26658	0.11740	0.03251
E_2	(a)	0.46525	0.25549	0.07326
	(b)	0.46418	0.25431	0.073186

$$E_1 = \frac{\sum_{x,y} \left[|u_1(x,y) - u_0(x,y)| |v_1(x,y) - v_0(x,y)| \right]}{\sum_{x,y} \left[|u_0(x,y)| + |v_0(x,y)| \right]} \quad (1)$$

$$E_2 = \frac{\sqrt{\sum_{x,y} \left\{ [u_1(x,y) - u_0(x,y)]^2 + [v_1(x,y) - v_0(x,y)]^2 \right\}}}{\sqrt{\sum_{x,y} \left\{ [u_0(x,y)]^2 + [v_0(x,y)]^2 \right\}}} \quad (2)$$

where u and v are the x and y components of the velocity and the subscripts 0 and 1 indicate the reference and the test case, respectively.

Since there is no analytic solution of the cavity flow the simulation with the 500×500 lattice has been taken as the reference case.

It is worth to highlight that flow velocities for different grids are taken at the same (corresponding) positions, while the sums are taken over the entire lattice.

The error values E_1 and E_2 are almost the same for LBGK and ELB simulation as demonstrated by the data summarized in Table ?? and plotted in Figure 1. As expected, a quadratic dependence of errors E_1 and E_2 on the lattice size is observed for both methods with grid sizes above 100×100 .

5. Viscosity analysis

In the entropic scheme, the parameter α (defined as the solution of the equation (12)) plays a central role, because of it gives the allowable limit in the updating step in order to obtain a local monotonic entropy function, in accordance with the H -theorem. Furthermore, the limit value of α establishes the maximal allowed value for the collision step along the direction defined by the vector Δ , as defined in equation (9), so that the entropy value will not decrease during the evolution of the phenomenon.

It is remarkable that a few changes to the entropic model let achieve the standard LBGK scheme, for example:

- looking at equation (22), it is clear that the condition $\alpha = 2$ allows us to recover the standard LBGK from the ELBM. It may be obtained simply by replacing $(1/\tau)$ with $(2 \cdot \beta)$;

However, the ELBM local equilibria differ widely from the LBGK ones. In particular, the ELBM equilibria go negative at higher values of the flow speed u . This is the feature of all isothermal models.

The departure of the entropic scheme from the LBGK condition can be characterized by the “entropic correction” parameter:

$$\epsilon = \alpha - 2. \quad (1)$$

If we consider the viscosity value $\nu_0 = \nu$, with $(\alpha = 2)$, as a reference:

$$\nu_0 = c_s^2 \cdot \left(\frac{1}{2\beta} - \frac{1}{2} \right) = \frac{c_s^2}{2} \cdot \left(\frac{1}{\beta} - 1 \right), \quad (2)$$

the ratio between effective viscosity ν and reference viscosity ν_0 , Δ_0 , can be taken as a measure of the local viscosity stabilization factor:

$$\Delta_0 = \frac{\delta\nu}{\nu_0} = \frac{(\nu - \nu_0)}{\nu_0} = -\frac{\epsilon}{(\epsilon + 2)} \frac{1}{(1 - \beta)}. \quad (3)$$

From a direct numerical observation, we know that $\epsilon \cong 0$ is vanishing and, as a consequence, the parameter Δ_0 can be approximated as follows:

$$\Delta_0 \cong -\frac{\epsilon}{2} \frac{1}{(1 - \beta)} = \frac{\epsilon}{2} \frac{1}{(\beta - 1)}. \quad (4)$$

We plot the value and the variation of this index in some histograms. In particular, figure 1 shows the Δ_0 spectrum of values at two different time steps and figure 2 shows the spatial

Reynolds	β	ν_0
400	0.8696	$2.49 \cdot 10^{-2}$
1000	0.9434	$1.0 \cdot 10^{-2}$
2000	0.9709	$4.9 \cdot 10^{-3}$
5000	0.9881	$1.9 \cdot 10^{-3}$
7500	0.9921	$1.3 \cdot 10^{-3}$

distribution of ϵ .

An accurate study of all these plots let deduce the following remarks:

- the viscosity correction Δ_0 shows minor departure from 0 for most of the nodes;
- most values of Δ_0 are positive, thus leading to a mean local viscosity greater than standard LBGK viscosity. Nonetheless, a significant fraction of $\Delta_0 < 0$ events are also observed. This is interesting, for it indicates that compliance with the H-theorem implies occasional *negative* diffusion corrections to the bare viscosity;
- the number of nodes where $\alpha \neq 2$ slightly increases with time, even though the shape of the spectrum remains almost the same;
- although the parameter ϵ takes very small values, i.e. it can be pinpointed in the range $[-0.0483, 0.0337]$, the correction to the local viscosity is significant;
- substantial departures are located around critical flow regions (i.e. close to the corners);

The above observations form the basis for the optimization strategies discussed in the next section.

6. Performance analysis and optimization

The simulation of a flow field through the ELB scheme requires a root finder evaluation at each time step, in order to compute the value of the parameter α that nullify the following G function:

$$G(\alpha) \equiv H(\mathbf{f}) - H(\mathbf{f} + \alpha \mathbf{\Delta}), \quad (1)$$

where $\mathbf{f} = (f_0, \dots, f_8) \in R^9$ is the population along the lattice vectors, $H(\mathbf{f})$ as defined in equation (6), w_i are the weight associated to the D2Q9 lattice, f_i^{eq} is the entropic mass distribution function, as defined in (8) and, finally,

$$\mathbf{\Delta} = \{\Delta_i = (f_i^{eq} - f_i), i = 0, \dots, 8\} \in R^9. \quad (2)$$

These just mentioned reasonings, let understand that at each time step and at each lattice site, a non-linear equation must be solved.

All the numerical simulations, realized in our research, make use of a modified Newton-Raphson method (i.e. coupled with a bisection procedure that provides higher stability at the zero finder) in order to solve the root evaluation question, as suggested by Karklin et al. in [24] and in [6].

With this strategy up to 8 steps are necessary for each root finder evaluation (this is consistent with the data and the estimations given by Karlin et al. in [24]).

These data clearly show that a bare application of the ELBM is computationally much more expensive than the standard LBGK method, and the computational effort grows directly with the size of the grid.

Therefore, the use of some kind/sort of optimization procedures seems to be a necessary task. These optimization strategies were developed and, in the following sections, the investigation of their effects, in terms of computational costs, accuracy and stability are given.

6.1. Optimization methodologies

In this section we are going to see some optimization strategies that were studied and realized in order to make ELBM an efficient tool as well. Really, all the methodologies have been realized and applied to a specific test case, i.e. the lid driven cavity flow problem, already used and largely described in previous sections, and are (in part) strictly dependent on-upon it.

It is known (as described by Karlin et al. in their papers and how it is easy to infer from the model description) that the entropic version of the lattice Boltzmann scheme requires a very heavy computational effort. For this reason it is becoming necessary that the attention for the optimization was directed towards different directions, not only related to the code implementation and to the programming tool optimization.

All the optimizations have been developed starting from a detailed investigation into the variation on the cavity of the parameters described previously, that is ϵ and Δ_0 . They can be summarized as follows:

1. search of an optimal starting point for the root finder. Indeed it is known that the Newton method is sensitive to choice of the starting point;
2. exclude from the computation of the updating parameter α (making use of the starting point $\alpha = 2$ in the root evaluation) all those sites that satisfy the following condition on the parameter Δ_0 :

$$|\Delta_0| < \Delta_{min}. \quad (3)$$

The value we consider to be as a good approximation of the real value, i.e. close to the value computed by the Newton-Raphson procedure. In the simulations is $\Delta_{min} = 10^{-3}$.

3. limit the computation of the parameter α to some critical regions located on the computational domain (as shown in Figure 1), for example where instability arises or where the computations are difficult to do. Out of these regions the value of α is fixed at 2.

This particular condition and strategy is strictly connected to the problem under consideration and to the geometry of the computational domain.

In the following sections an accurate description of the optimization strategies is given, trying to focus the attention on effects on the numerical results.

6.2. Optimal starting point for the root finder

The Newton-Raphson procedure has a local second order convergence rate. In spite of this, its global convergence properties are poor. For this reason a suitable choice of the starting point for the root finder evaluation is a crucial task to find the solution/zero of the function with the Newton method.

Therefore since the function we have to evaluate is monotonic and the variation rate is very slow, the use of a suitable starting point could give a substantial and important computational saving.

Furthermore, verified that

- the solution of equation (1) is very close to 2, by the investigation of the parameter Δ_0 described in section 5;
- just a little departure from this reference value gives a significant improvement in the stability of the kinetic model;
- the departure rate from the initial value 2 is connected to the position on the computational domain, as discussed by the investigation of the parameter ϵ in section 5.

These reasoning and remarks let us pursue the idea that the starting point α_0 for the root finder procedure have to be close to the reference value 2. An improving strategies and choice could be given by taking α_0 at the computational time t equal to the value computed in the same site at previous time step.

This let us use and implement the following procedure:

$$\alpha_{x,y}^t = \begin{cases} \alpha_{x,y}^{t-\delta t}, & t > 0, \\ 2, & t = 0, \end{cases} \quad (4)$$

where $\alpha_{x,y}^t$ is the starting point for the Newton-Raphson procedure at the time t and $\alpha_{x,y}^{t-\delta t}$ is the solution of equation (1) at the time $t - \delta t$.

With this simple recipe, the maximum number of steps, necessary to find the solution of the equation (1), has been reduced from 8 to 5, thus reducing significantly the computational costs.

6.3. Control on the variation of the local viscosity

Another important observation about the optimization of the performance, arises from the analysis about the variation of the local viscosity value on the site of the computational domain. Indeed, as shown in Figures 1 and 2, it has been observed that, except for restricted critical zones, Δ_0 is very close to 0 (for the cavity flow at $Re = 5000$ its order is about 10^{-3} , from an experimental observation).

Therefore, assuming that in those sites where Δ_0 is below a certain threshold, the stability would be guaranteed even by applying the LBGK collision instead of the stabilized one.

In order to test this technique, the simulations on the cavity have been repeated by computing dynamically the updating parameter α only at those sites where $\Delta_0 > 10^{-3}$ and setting $\alpha = 2$

elsewhere. This technique lets the simulation being still performed at $Re = 5000$ ^g.

Furthermore the investigation and the observation of some kind of qualitative and quantitative data, as the velocity profiles and the stream function, let us conclude that the applied optimization procedure do not effect the accuracy of the model.

As shown in Figure 2, the stream function distribution is almost the same as for the standard ELB method. This is confirmed by the longitudinal and transverse velocity profiles, which give a most accurate quantitative measure. As shown in Figure 3, the data obtained by this optimization strategy are perfectly superimposed to those of the standard ELB method.

6.4. Geometrical optimization: definition of critical regions

All the optimization strategies applied and described previously, are free from any connection with the geometrical and physical characteristic of the problem and the simulation. This means that the technique could be applied also a priori without any definition or knowledge of the flow problem.

The optimization technique we are going to describe in this section, instead, is strictly tied with the problem definition, i.e. the specification of both, the geometrical and flow features.

In the special case of the lid driven cavity flow, described and studied in our research and in literature, it is well known that the major problems occur around the four corners. In these regions the computation is highly critical, especially the upper ones (as shown in Figure 1), where the velocity is imposed.

In addition, the results obtained by the investigation on the parameter ϵ (as in section 5 and in Figures 2) highlight the major and fundamental work of the entropic model around the upper corners. So the exclusion from the computation of the updating parameter α in all the other parts of the domain may be assumed.

So some simulations were performed assuming to restrict the entropic formulation and computation of the kinetic method into the regions considered as critical.

In this way all those regions located outside the *critical* zones are skipped from the use of the entropic method and from the computation of the parameter α , whose value is assumed be equals to 2.

In order to numerically identify those regions we considered two sector of a circle centered in the upper corners, whose rays are r_1 and r_2 , as in Figure 1.

The simulations performed in order to evaluate the accuracy and the goodness of the idea just described, were realized considering three different values of the two circles radius:

$$R = r_1 = r_2 \in \{0.25L, 0.4L, 0.5L\}, \quad (5)$$

where L is the length of the cavity side.

The evaluation of the accuracy of this optimization strategy (likewise done in previous paragraph) is realized considering both the plot of the stream function (as in Figure 4) and the plot

^gThis is a lucky sign of success.

of the longitudinal and transverse velocity profiles (as in Figure 5).

The qualitative and quantitative data show a good agreement with the standard ELB methods

6.5. Computational saving evaluation

In previous paragraphs we describe the optimization strategies that could be applied to the entropic model in order to have a computational saving and estimate the accuracy and reliability of the results that they give. Here we evaluate and quantize the effective computational saving, that is significant, obtained by applying these optimization methods.

Taking the LBGK simulation as the reference one, in order to study the computational cost of ELBM compared to LBGK, we define the parameter $\Upsilon(t)$ as follows:

$$\Upsilon(t) = \frac{T_{ELB}(t)}{T_{BGK}(t)}, \quad (6)$$

where $T_{ELB}(t)$ and $T_{BGK}(t)$ are the cpu time per time step of ELB and LBGK method at time t respectively. The parameter $\Upsilon(t)$ is plotted in Figure 6. Here all the values of $\Upsilon(t)$ are compared, i.e. the ones computed by the application of ELBM with all the optimization strategies described.

Looking at the plot of $\Upsilon(t)$, the following observations may be done:

- the simulation of the cavity flow with the ELB method costs nearly three times as much as the standard LBGK (curve *a*);
- skipping the α calculation where $\Delta_0 < 10^{-3}$, allows to save about 20% of the computational costs (curve *b*) and an additional 5% is recovered by simply changing the starting point (curve *c*);
- another significant saving (curves *d*, *e* and *f*) is obtained by restricting the system computation only to “a priori” chosen regions of the domain, where it is supposed (in this case, it is known) that the computation is critical;
- by limiting the calculation of α to two identical sectors of a circle around the upper corners (see fig. 1) with radius $R = 0.25$, one obtains a computational costs comparable (1.5times) with standard LBGK.

7. ELB as a sub-grid model

The discussion done in previous sections allow us to prise the entropic model for the capability of reliably computing large-scale structures (e.g. primary and secondary vortices in the present case) even in conditions where the small-scale features of the flow are not resolved by the grid. The optimization strategies studied in previous section 6.1 show that all these advantages are almost free of extra computational charges.

These aforementioned characteristics are the chief requirements on a “good” sub-grid model for turbulent flows.

It is therefore of interest to discuss a little bit deeper the analogies between ELB and kinetic turbulence models, as done by Ansumali, Karlin and Succi in [36].

The latter schemes are currently implemented by adding a self-consistent turbulent time-scale, τ_t , to the bare molecular one, τ_0 :

$$\tau = \tau_0 + \tau_t. \quad (1)$$

For fully developed turbulence, the turbulent timescale normally satisfies the condition $\tau_t \gg \tau_0$. By comparing expressions (1) and (3), we may observe that

$$\delta\nu/\nu_0 \sim \tau_t/\tau_0. \quad (2)$$

From this equation, we can conclude that for the present case ELB corrections are of the same order of the bare relaxation time. This conclusion is by no means a general one, and should be investigated further by analyzing fully developed turbulent flows with ELB.

A second observation is that, at variance with kinetic turbulence models, τ_t is allowed to take on *negative* values, associated to local instabilities. The role of these ‘negative-viscosity’ events remains to be clarified and will make the object of future investigations.

REFERENCES

1. J. Connor and C. Brebbia, Finite element techniques for fluid flow, *Newnes-Butterworths*, 1976.
2. J. Dupuy and A. Dianoux, Microscopic structure and dynamics of liquids, *Plenum Press*, 1978.
3. U. Frisch and B. Hasslacher and Y. Pomeau, Lattice-gas automata for the Navier-Stokes equation, *Phys. Rev. Lett.*, **56**, (1986), pp. 1505 – 1508
4. S. Succi, The Lattice Boltzmann Equation for fluid dynamics and beyond, *Claredon press*, Oxford University Press, (2001)
5. S. Ansumali, Minimal kinetic modelling of hydrodynamics, *PhD Thesis*, No 15534, ETH Z’urich, (2004).
6. S. Ansumali and I.V. Karlin, Stabilization of the lattice Boltzmann method by the *H*-theorem: A numerical test, *Phys. Rev. E*, **62**(6), (2000), pp.7999-8003.
7. S. Ansumali and I.V. Karlin, Single relaxation time model for entropic lattice Boltzmann methods, *Phys. Rev. E*, **65**, (2002), pp.056312.
8. S. Ansumali and I.V. Karlin and H.C.Öttinger, Minimal entropic kinetic models for hydrodynamics, *Europhys. Lett.*, **63**(6), (2003), pp. 798-804.
9. Erturk E. and T.C. Corke and C. G..., Numerical solutions of 2-D steady incompressible driven cavity flow at high Reynolds numbers, *Int. J. Num.Methods in Fluid*, **48** (7), (2005), pp.747 - 774.
10. S. Hou and Q. Zou and S. Chen and G. Doolen and A. C. Cogley, Simulation of cavity flow by the lattice Boltzmann method, *J. of Comp. Phys.*, **11**, (1995), pp. 329-347.
11. Y. Li and R. Shock and R. Zhang and H. Chen, Numerical study of flow past an impulsively started cylinder by the lattice-Boltzmann method, *Journal of Fluid Mech.*, **519**, (2004), pp. 273–300.
12. U. Frisch and D. d’Humières and B. Hasslacher and P. Lallemand and Y. Pomeau and J.P. Rivet, Lattice gas hydrodynamics in two and three dimensions, *Complex Systems*, **1**, (1987), pp. 649.

13. A. K. Gunstensen and D. H. Rothman, A Galilean-invariant immiscible lattice gas., *Physica D*, **47**, (1991), pp. 53 – 63
14. D. d' Humières, P. Lallemand, and G. Searby, Numerical experiments on lattice gases: Mixtures and Galilean invariance., *Complex Systems*, **1**, (1987), pp. 633 – 647.
15. G. McNamara and G. Zanetti, Use of the Boltzmann equation to simulate lattice gas automata, *Phys. Rev. Lett.*, **61**, (1988), 2332.
16. F. J. Higuera and J. Jimenez, Boltzmann approach to lattice gas simulations, *Europhys. Lett.*, **9**, (1989), pp. 663.
17. P. L. Bhatnagar and E. P. Gross and M. Krook, A model for collision processes in gases. I. Small amplitude processes in charged and neutral one-component system, *Phys. Rev.*, **94**, (1954), pp. 511-525.
18. S. Chen, H. Chen, D. Martinez and W. H. Matthaeus, Lattice Boltzmann model for simulation of magnetohydrodynamics, *Phys. Rev. Lett.*, **67**, (1991), pp. 3776 – 3779.
19. J. M. Koelman, A simple lattice Boltzman scheme for Navier-Stokes fluid flow., *Europhys. Lett.*, **15(6)**, (1991), pp. 603.
20. Y.H. Qian and D. d'Humieres and P. Lallemand, Lattice BGK models for Navier-Stokes equation, *Europhys. Lett.*, **17**, (1992), pp. 479-484.
21. P. J. Love and B. M. Boghosian, On the dependence of the Navier - Stokes equations on the distribution of molecular velocities, *Phys. A*, **332**, (2004), pp. 47 - 59.
22. H. Chen, S. Chen and W. H. Matthaeus, Recovery of the Navier-Stokes equations using a lattice-gas Boltzmann method, *Phys. Rev. A*, **45**, (1992), pp. 5339 – 5342.
23. F. J. Higuera and S. Succi and R. Benzi, Lattice gas dynamics with enhanced collisions, *Europhys. Lett.*, **9**, (1989), pp. 345-349.
24. S. Ansumali and I. V. Karlin, Entropy Function Approach to the Lattice Boltzmann Method, *J. of Stat. Phys.*, **107**, (2002), pp. 291.
25. I.V. Karlin and A. Ferrante and H.C.Öttinger, Perfect entropy functions of the Lattice Boltzmann method, *Europhys. Lett.*, **47(2)**, (1999), pp. 182-188.
26. I. V. Karlin and A. N. Gorban and S. Succi and V. Boffi, Maximum entropy principle for Lattice Kinetic equations, *Phys. Rev. Letters*, **81**, (1998), pp. 6-9.
27. B.M. Boghosian and J. Yepez and P.V. Coveney and A.J. Wagner, Entropic Lattice Boltzmann Methods, *Proc. R. Soc. London, Ser. A* , **457**, (2001), pp. 717.
28. I.V. Karlin and S. Succi, Equilibria for discrete kinetic equations, *Phys. Rev. E*, **58**, (1998), pp. 4053.
29. A. Wagner, An H-theorem for the lattice Boltzmann approach to hydrodynamics, *Europhys. Lett.*, **44**, (1998), pp. 144.
30. A.N. Gorban, I.V. Karlin, V.B Zmievskii and T.F Nonnenmacher, Relaxation trajectories: global approximations, *Physica A*, **231**, (1996), pp. 648-672.
31. H. Grad, On the Kinetic Theory of Rarefied Gases, *Commun. Pure Appl. Math.*, **2**, (1949), pp. 331.
32. X. Shan and X. He, Discretization of the Velocity Space in the solution of the Boltzmann equation, *Phys. Rev. Lett.*, **80(1)**, (1998), pp. 65-68.
33. F. Tosi and S. Ubertini and S. Succi and H. Chen and I.V. Karlin, A comparison of single-time relaxation lattice Boltzmann schemes with enhanced Stability, *International Journal of Modern Physics C*, **10(17)**, (2006), pp. 1 - 16.

34. [F. Tosi and S. Ubertini and S. Succi and H. Chen and I.V. Karlin, Numerical stability of Entropic versus positivity-enforcing Lattice Boltzmann schemes, *Mathematics and Computers in Simulation*, **10.1016**, \(2006\).](#)
35. [F. Tosi and S. Ubertini and S. Succi and I.V. Karlin, Optimization strategies for the entropic lattice Boltzmann method, *Journal of Scientific Computing*, \(2006\).](#)
36. [S. Ansumali and I.V. Karlin and S. Succi, Kinetic theory of turbulence modeling: smallness parameter, scaling and microscopic derivation of Smagorinsky model, *Physica A*, **337**, pp. 379–394, \(2004\).](#)

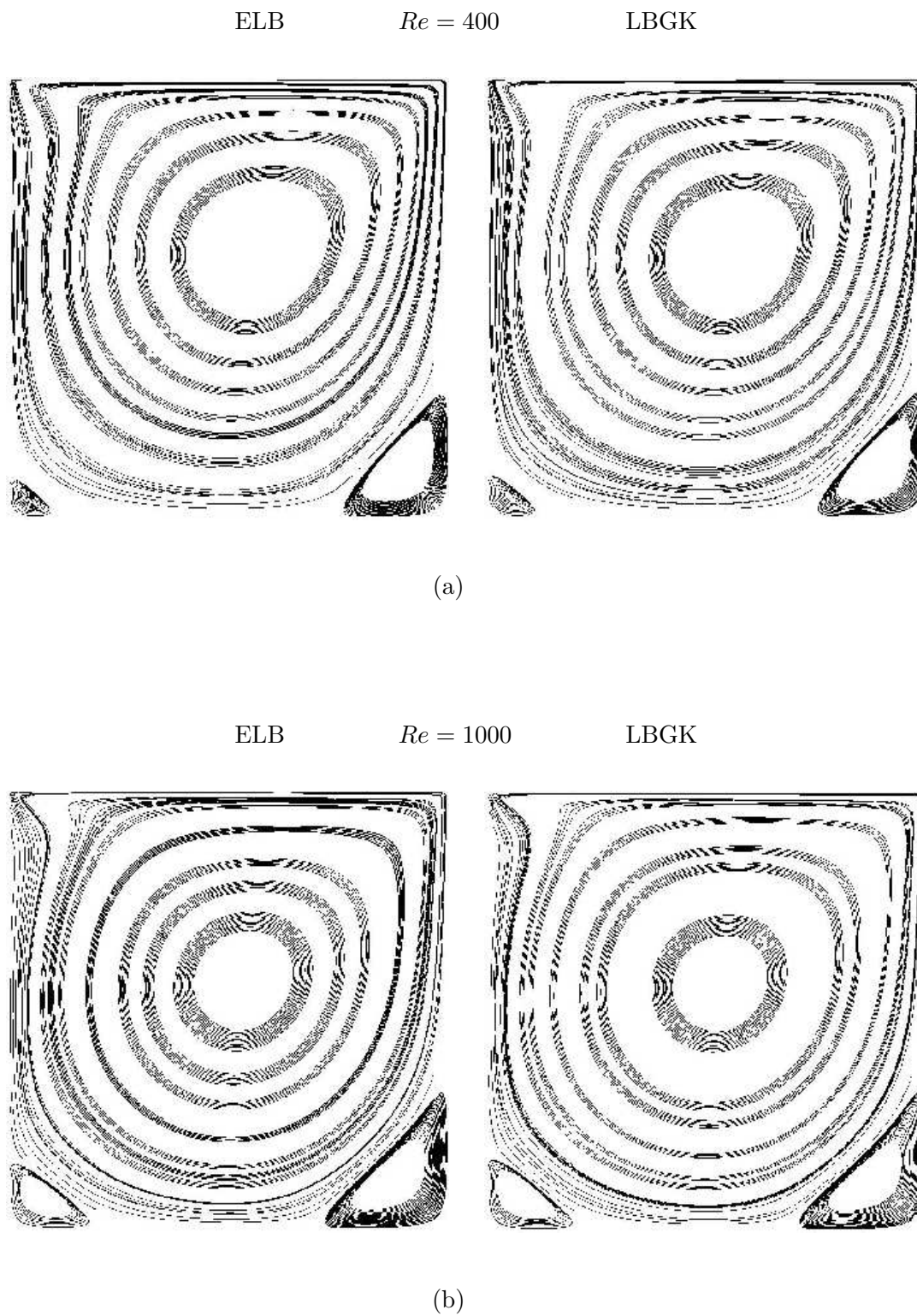


Figure 5. Stream function for the cavity flow simulation: on the left side plot obtained with a simulation based on ELBM, on the right side plot with a LBGK based simulation. The top velocity \mathbf{u} is set to $\mathbf{u} = (0.1, 0)$. 100×100 grid and the Reynolds number is $Re = 400$, in (a), and $Re = 1000$.

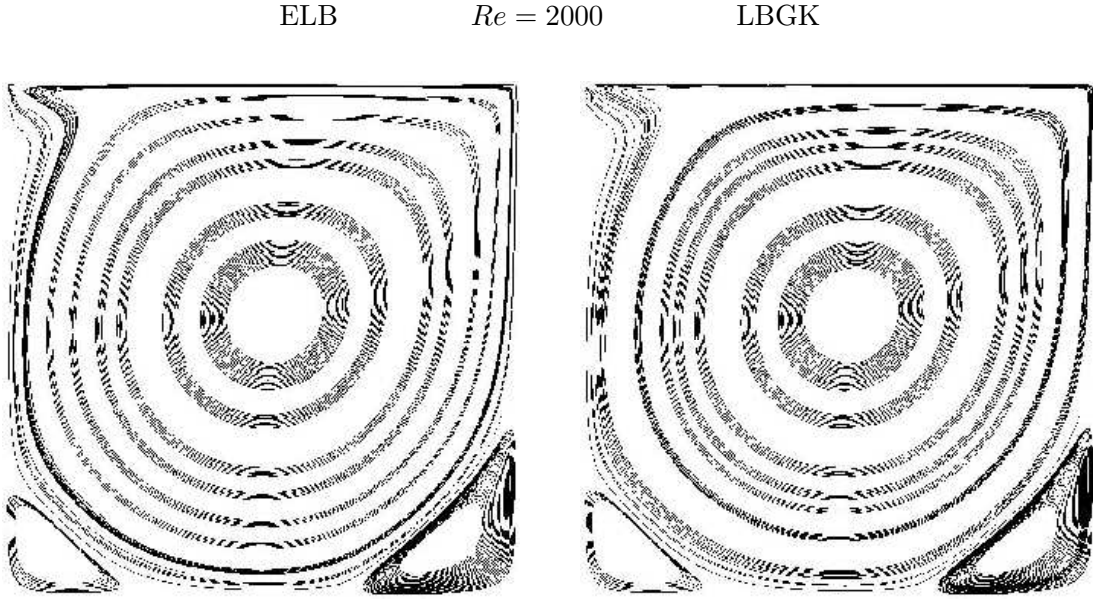


Figure 6. Stream function: on the left side plot obtained with a simulation based on ELBM, on the right side plot with a LBGK based simulation. The top velocity \mathbf{u} is set to $\mathbf{u} = (0.1, 0)$. 100×100 grid and the Reynolds number is 2000.

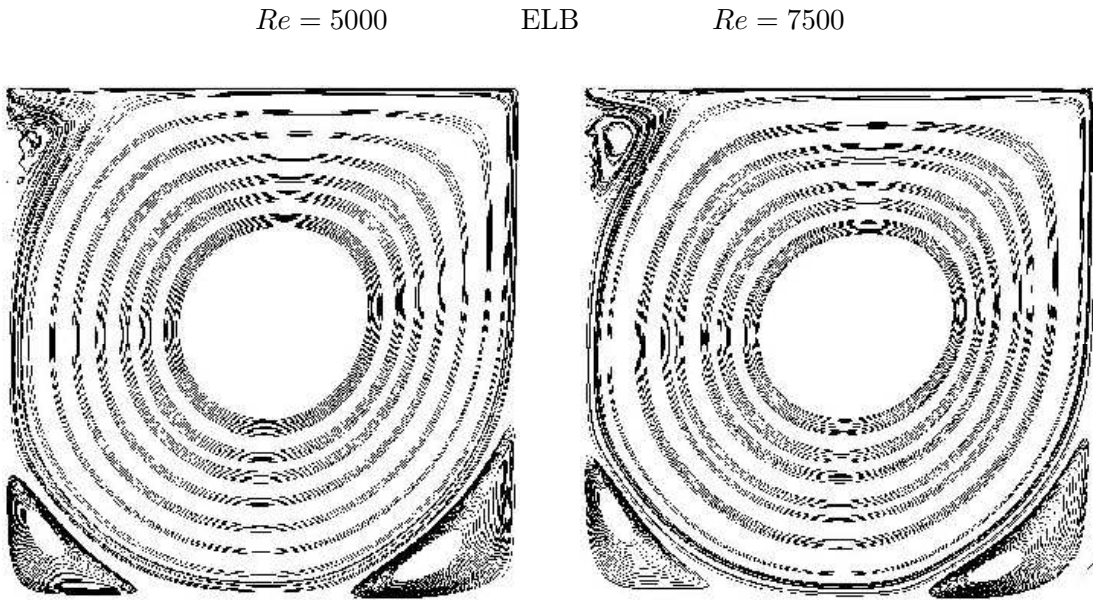


Figure 7. Stream function with ELB. Top velocity $\mathbf{U} = (0.1, 0)$. 100×100 grid. Reynolds numbers 5000 (left) and 7500 (right). For these values of Re and with this grid resolution the LBGK simulation fails.

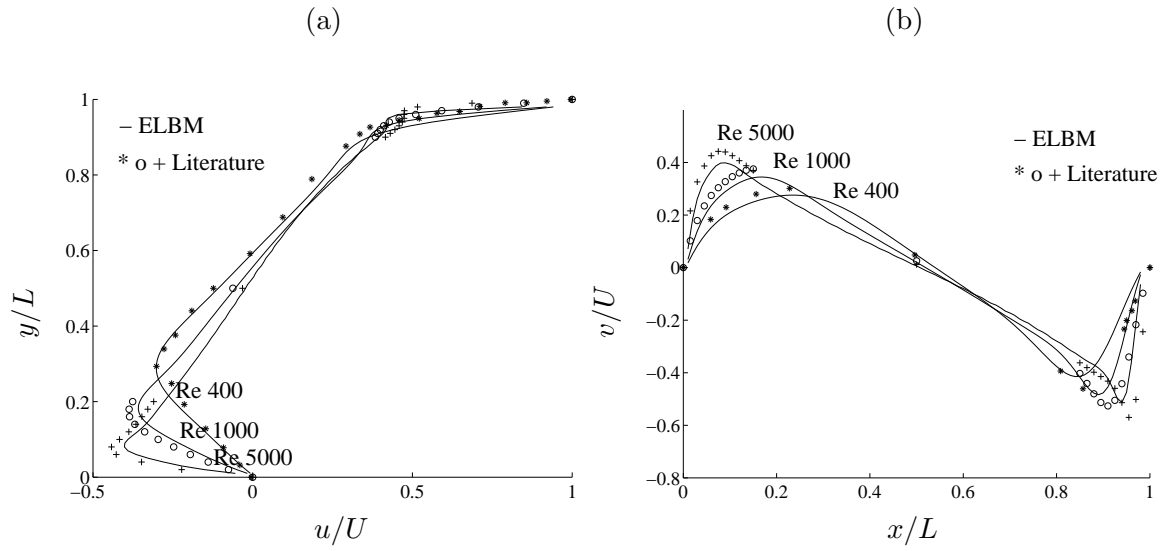


Figure 8. Profile of the longitudinal in (a) and transverse in (b) velocities u, v at the centreline $x = L/2$ - Comparison with literature data, cfr. Erturk et al. in [9] (scatter points).

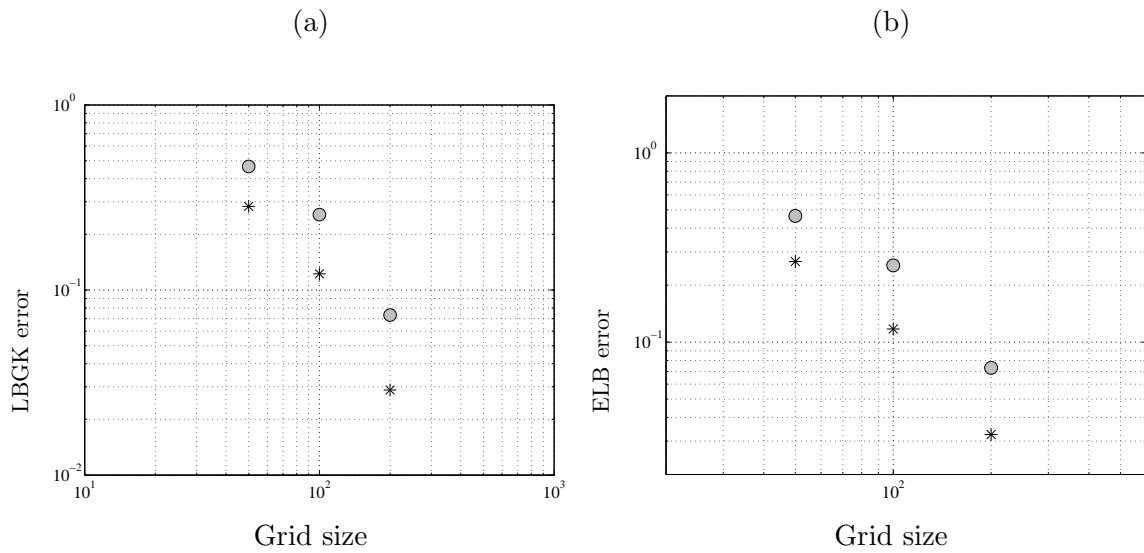


Figure 1. Plots (on a logarithmic scale) of the error E_1 (circles) and E_2 (stars) in the simulations realized by LBCK model in (a) and by ELBM.

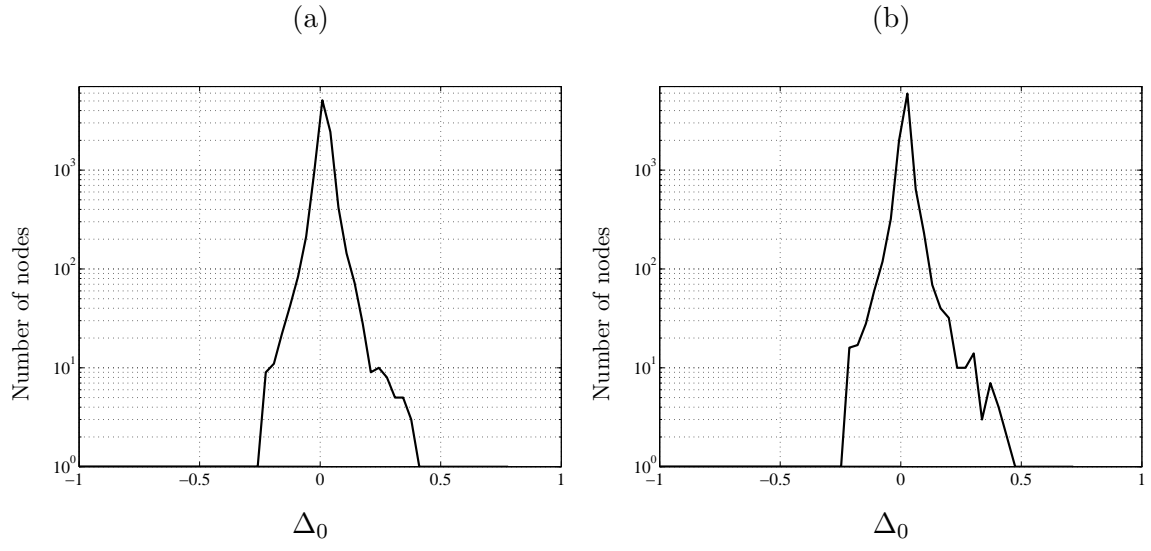


Figure 1. The distribution of the parameter Δ_0 at $t = 12500$ (a) and $t = 65000$ (b).

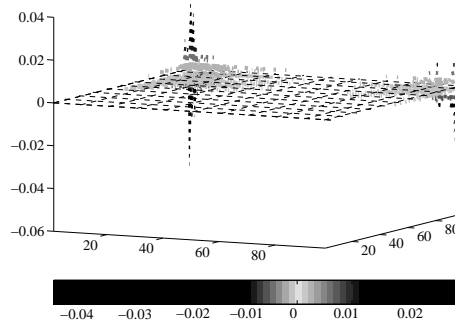


Figure 2. The distribution of the parameter ϵ at $t = 65000$.

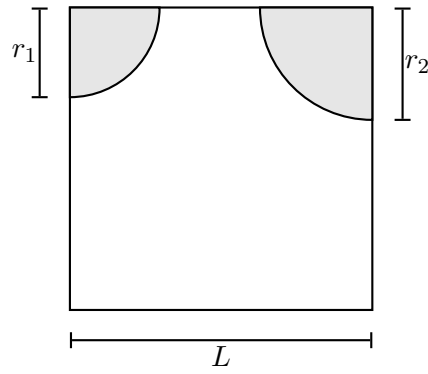


Figure 1. Critical regions of the numerical flow simulation on a cavity with a moving upper side.

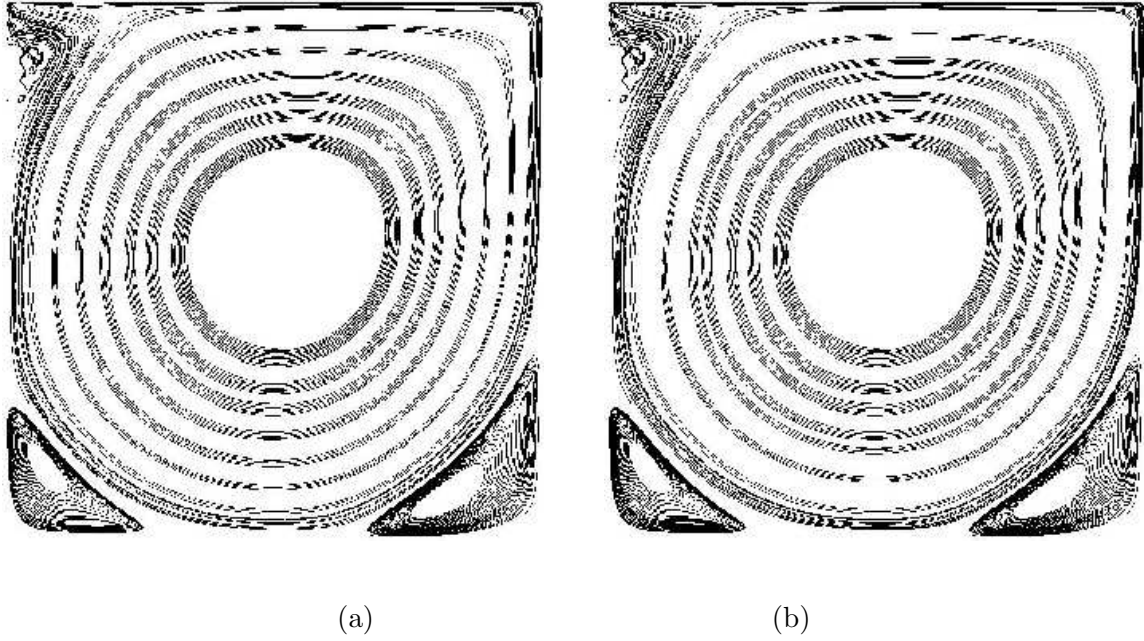


Figure 2. Stream-function for $Re = 5000$, top-velocity $\mathbf{u} = (0.1, 0)$, after 65000 time steps (a) standard ELB model, (b) ELB with a dynamic computation of the parameter α , restricted in all those site where $\Delta_0 > 10^{-3}$. The grid size is 100×100 .

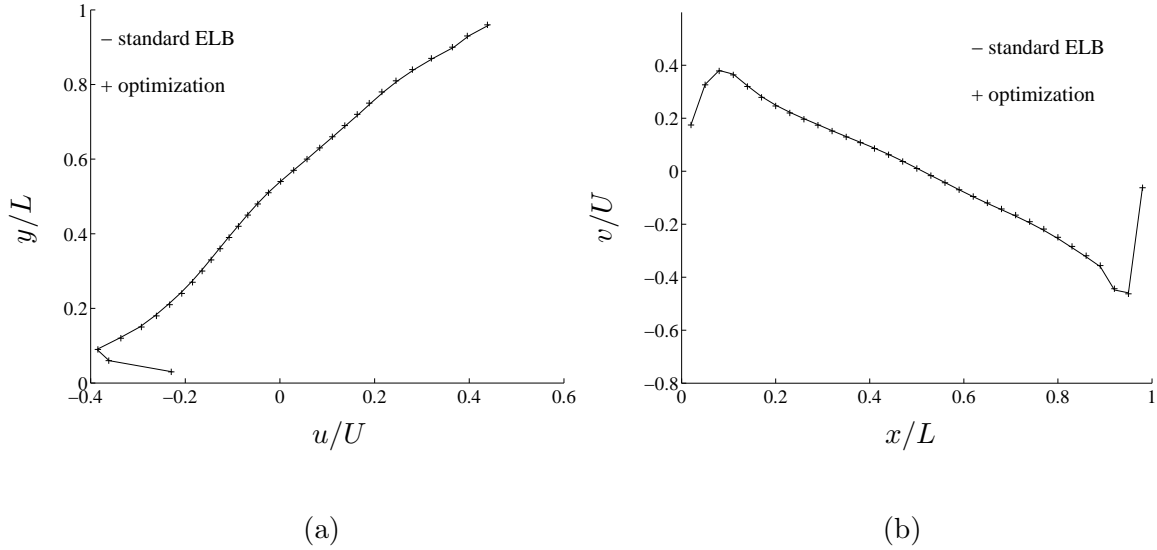


Figure 3. Longitudinal and transverse velocity profiles at the centreline $x = L/2$ for $Re = 5000$; dashed line - standard ELB, solid line - ELB with α computation only where $\Delta_0 > 10^{-3}$.

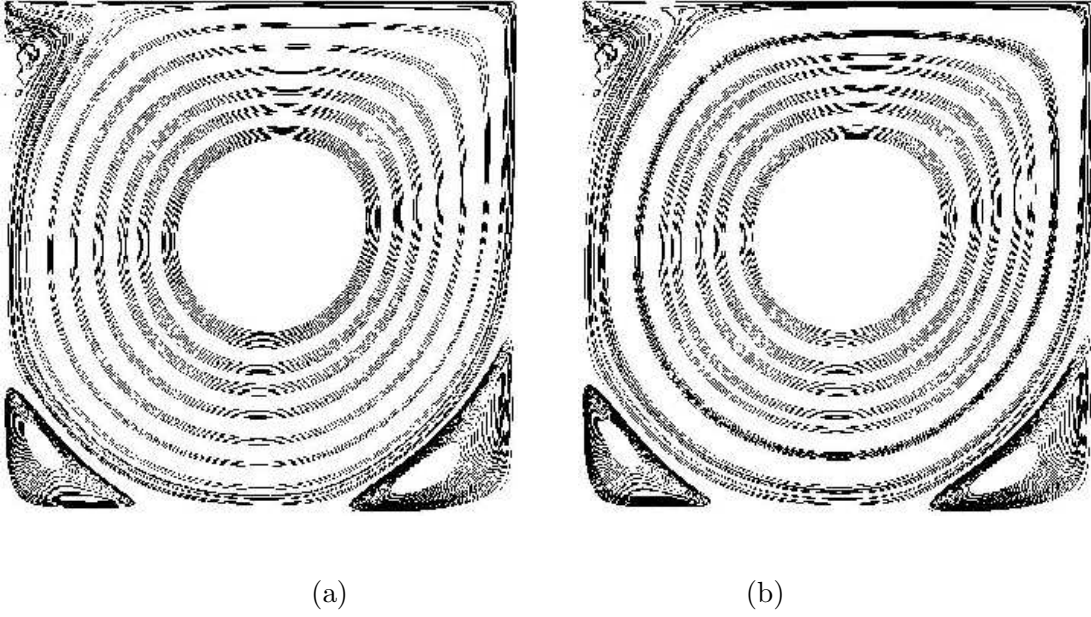


Figure 4. Stream function for $Re = 5000$, top velocity $\mathbf{u} = (0.1, 0)$, after 65000 time steps: (a) standard ELB model, (b) ELB with a limitation of the computation of the parameter α in a restricted areas around the upper corners (see fig. 1, using a radius $R = 0.25 \cdot L$). The grid size is 100×100 .

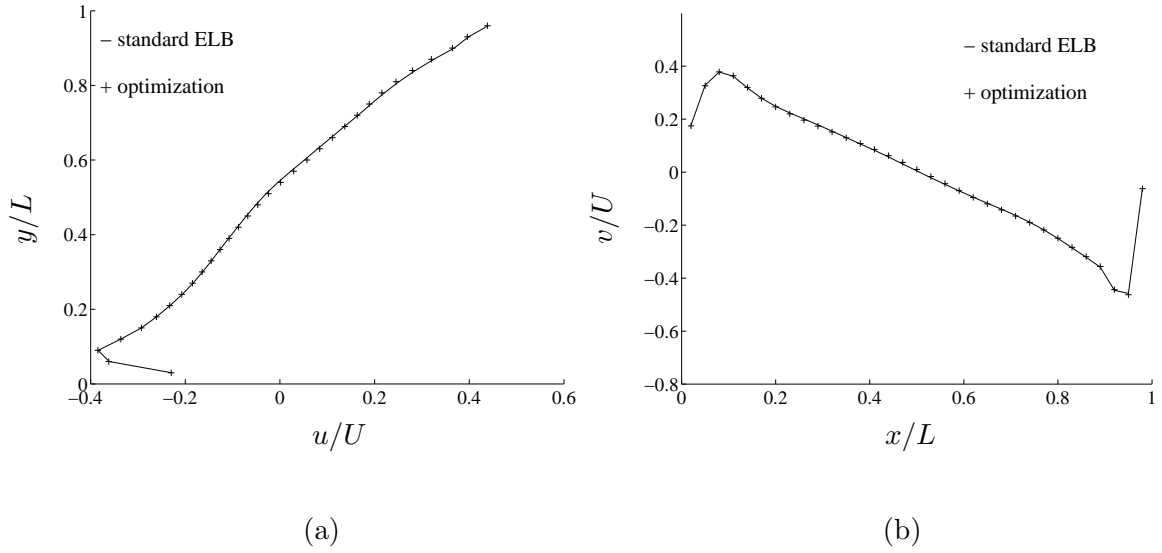


Figure 5. Longitudinal and transverse velocity profiles at the centreline $x = L/2$ for $Re = 5000$; dashed line - standard ELB, solid line - ELB with α computation limited in restricted areas around the upper corners (see fig. 1 with $R = 0.25 \cdot L$)

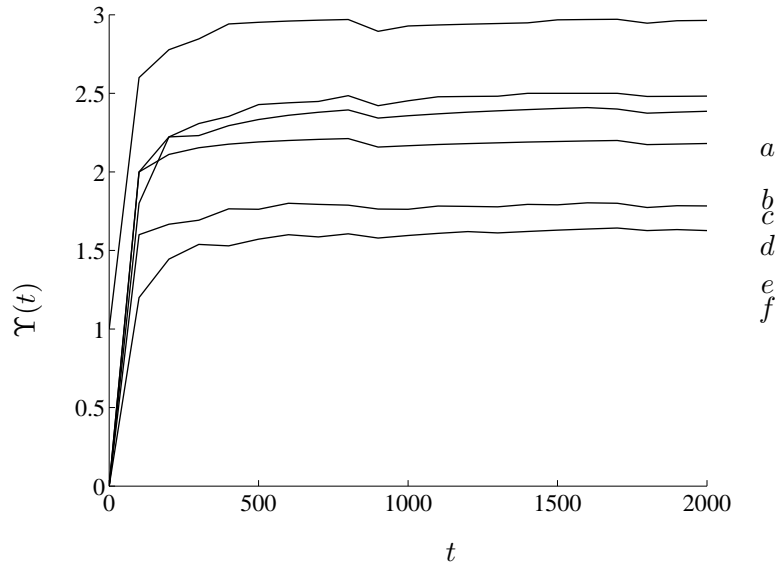


Figure 6. Plot of the quotient $\Upsilon(t)$, taken as a quantitative parameter to evaluate the cpu time of the entropic model and to compare with the LBGK scheme. It is plotted considering the cpu time of the standard entropic model (a) and all the optimization strategies described, i.e.: (b) Optimal Newton-Raphson starting point, (c) α calculation skipped where $\Delta_0 < 10^{-3}$, (d), (e) and (f) α calculation restricted to two identical sectors of a circle around the upper corners with radius $R = 0.5 \cdot L$, $R = 0.4 \cdot L$ and $R = 0.25 \cdot L$, respectively.